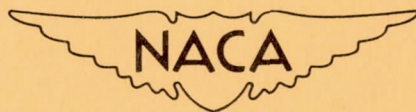# NATIONAL ADVISORY COMMITTEE
FOR AERONAUTICS

TECHNICAL NOTE 3938

SIDEWASH IN THE VICINITY OF LIFTING SWEPT WINGS

AT SUPERSONIC SPEEDS

By Percy J. Bobbitt and Peter J. Maxie, Jr.

Langley Aeronautical Laboratory
Langley Field, Va.

NACA

Washington

February 1957

NATIONAL ADVISORY COMMITTEE FOR AERONAUTICS

TECHNICAL NOTE 3938

SIDEWASH IN THE VICINITY OF LIFTING SWEPT WINGS

AT SUPERSONIC SPEEDS

By Percy J. Bobbitt and Peter J. Maxie, Jr.

SUMMARY

In order to calculate the induced loading on a store, missile, or
pylon situated in close proximity to a wing-fuselage combination, a
detailed knowledge of the flow field is required. The present paper
provides some of this needed information by presenting equations and
charts that enable the determination of sidewash in the vicinity of semi-
infinite triangular wings at small angles of attack. These results may
also be used directly in sidewash determinations for the conical part of
the flow exterior to wings having finite spans and chords. At points in
the flow field affected by the finite-wing wake or tip, additional con-
siderations are necessary to determine the sidewash. Both the subsonic-
wing and supersonic-wing leading-edge conditions have been treated; hence,
sidewash is obtainable for all supersonic Mach numbers and leading-edge
sweep angles for sweptback wings.

INTRODUCTION

The ever increasing use of external stores and missiles on aircraft
has emphasized the need for a method of predicting the loads acting on
these stores and missiles and also on the pylons by which they are often
attached to the wing. Store, missile, and pylon loadings are required
in designing the pylon structure, in predicting the lateral stability
of aircraft, in determining the jettison characteristics of stores, and
in computing the trajectories of missiles.

A number of experimental investigations have been conducted in the
past several years in an attempt to gain some insight into the origin
of store loads and, in a few isolated cases, pylon loads. Through system-
atic tests on the effects of store position, store size, wing plan form,
pylons of various types, and Mach number, the understanding of the various
interference effects has been increased. However, due to the many vari-
ables involved in the airplane-store or airplane-missile problem, there
remains a very definite need for an analytical or semiempirical method
capable of indicating trends (if not magnitudes) when the many variables
involved are changed.

One of the most important prerequisities to making a calculation of the store, missile, or pylon loading is a detailed knowledge of the flow field in the immediate vicinity of the wing. In reference 1 an extensive theoretical treatment of the pertinent flow fields at subsonic speeds has been presented, together with some experimental verification. At supersonic speeds the picture is not quite so complete. The longitudinal and vertical velocity components in the vicinity of the wing which are due to the wing angle of attack have been derived in references 2, 3, 4, and 5, and some information related to the velocity components in fuselage flow fields and wing-thickness flow fields may be extracted from references 6 and 7. The lateral flow velocity in the vicinity of the wing due to the wing angle of attack has not yet been treated.

The present paper is concerned with the latter, that is, the analytical determination of the lateral flow velocity (sidewash) in the vicinity of the wing due to the wing angle of attack. The methods used parallel the linearized lifting-surface methods employed in reference 3 to determine the downwash in the flow field exterior to flat lifting triangles of infinite chord. The analyses apply for all leading-edge sweep angles for sweptback wings and supersonic Mach numbers, both the subsonic-wing leading-edge and supersonic-wing leading-edge conditions being considered. It should be pointed out that the infinite-chord triangular-wing sidewash, which is derived herein, may also be used directly in sidewash determinations for some regions near wings having finite spans and chords. For points affected by the wing wake or wing tip, additional considerations are, of course, necessary (see ref. 5) and the expressions for the sidewash velocity given in the present paper represent only a part of the total sidewash. The results of the investigation are presented in chart form for various combinations of leading-edge sweep and Mach number.

SYMBOLS

The system of axes used in the analysis and the positive directions of the velocities are shown in figure 1.

b   span of triangular wing

C   constant of integration

c   root chord of triangular wing

E_i imaginary part of incomplete elliptic integral of second kind

E_r real part of incomplete elliptic integral of second kind

$E\left(\sqrt{1 - \beta^2 m^2}\right)$ complete elliptic integral of second kind with modulus $\sqrt{1 - \beta^2 m^2}$

$E(\omega, k)$ incomplete elliptic integral of the second kind with modulus k and sine amplitude ω, $\displaystyle\int_0^\omega \frac{\sqrt{1 - k^2 \omega_1^2}\, d\omega_1}{\sqrt{1 - \omega_1^2}}$

F_i imaginary part of incomplete elliptic integral of first kind

F_r real part of incomplete elliptic integral of first kind

$F(\omega, k)$ incomplete elliptic integral of first kind with modulus k and sine amplitude ω, $\displaystyle\int_0^\omega \frac{d\omega_1}{\sqrt{1 - \omega_1^2}\,\sqrt{1 - k^2 \omega_1^2}}$

I.P.   imaginary part

k modulus of elliptic integrals, $\sqrt{1 - s_0^4}$

k' comodulus of elliptic integrals, $k' = \sqrt{1 - k^2} = s_0^2$

M_∞ free-stream Mach number, $\dfrac{V_\infty}{\text{Velocity of sound in free stream}}$

m cotangent of sweep angle of wing leading edge

$p = \dfrac{\beta \dfrac{z}{x}}{1 + \sqrt{1 - \left(\dfrac{y}{x}\right)^2 - \left(\dfrac{z}{x}\right)^2}}$

$q = \dfrac{\beta \dfrac{y}{x}}{1 + \sqrt{1 - \left(\dfrac{y}{x}\right)^2 - \left(\dfrac{z}{x}\right)^2}}$

$$s_0 = \frac{1 - \sqrt{1 - \beta^2 m^2}}{\beta m}$$

u,v,w   perturbation velocities in x-, y-, and z-directions

V   complex sidewash function, $v + i\bar{v}$

V_∞ free-stream velocity

$\bar{v}$ harmonic conjugate of v

x,y,z   Cartesian coordinates of field point with origin at wing
                 apex (the positive directions are indicated in fig. 1)

α angle of attack, radians

$$\beta = \sqrt{M_\infty^2 - 1}$$

δ imaginary part of a complex variable

ζ complex variable, $\zeta = p + iq = \dfrac{\beta \dfrac{z}{x} + i\beta \dfrac{y}{x}}{1 + \sqrt{1 - (y/x)^2 - (z/x)^2}}$

$\lambda = sn^2(F_r, k)$

μ complex incomplete elliptic function of first kind (real
                 part is given by μ_r and imaginary part by μ_i)

ξ, η complex variables

$\sigma = sn^2(F_i, k')$

τ real part of a complex variable

ϕ perturbation-velocity potential

Subscripts:

1   refers to complex variable ξ

2   refers to complex variable η

i   refers to imaginary part of a complex function

r   refers to real part of a complex function

PRESENTATION OF SIDEWASH EQUATIONS

The methods used in reference 3 for the determination of the down-wash in the flow fields exterior to flat lifting triangular wings of infinite chord may also be used for the determination of the sidewash in the flow fields exterior to these same wings. For this reason, this section will be restricted primarily to the presentation of the sidewash equations with the actual derivations given in appendixes A and B.

Sidewash equations presented will apply directly for points below the right-hand panel of the wing; however, since the sidewash is anti-symmetric with z (i.e., about the plane of the wing) and y, the signs on the equation may be changed to give the sidewash for any point in the field.

Subsonic-Leading-Edge Wing

The sidewash at a point (x,y,z) below the right-hand panel of the lifting triangular wing, as developed in appendix A, is given by

$$v = \frac{V_\infty \alpha}{\left(1 - s_0^2\right) E\left(\sqrt{1 - \beta^2 m^2}\right)} \left\{ -E\left(\sqrt{\sigma_1}, s_0^2\right) + \frac{\left[1 - \left(1 - s_0^4\right)\lambda_1\right]\sqrt{\sigma_1}\sqrt{1 - \sigma_1}\sqrt{1 - s_0^4\sigma_1}}{1 - \left[1 - \left(1 - s_0^4\right)\lambda_1\right]\sigma_1} + E\left(\sqrt{\sigma_2}, s_0^2\right) - \frac{\left[1 - \left(1 - s_0^4\right)\lambda_2\right]\sqrt{\sigma_2}\sqrt{1 - \sigma_2}\sqrt{1 - s_0^4\sigma_2}}{1 - \left[1 - \left(1 - s_0^4\right)\lambda_2\right]\sigma_2} \right\} \tag{1}$$

where

$$s_0 = \frac{1 - \sqrt{1 - \beta^2 m^2}}{\beta m}$$

In order to calculate the λ and σ functions in equation (1), proceed as follows. First, calculate p and q:

$$p = \frac{\beta \frac{z}{x}}{1 + \sqrt{1 - \left(\beta \frac{y}{x}\right)^2 - \left(\beta \frac{z}{x}\right)^2}} \tag{2}$$

$$q = \frac{\beta \frac{y}{x}}{1 + \sqrt{1 - \left(\beta \frac{y}{x}\right)^2 - \left(\beta \frac{z}{x}\right)^2}} \tag{3}$$

and then calculate τ_1, δ_1, τ_2, and δ_2:

$$\tau_1 = \left[p\sqrt{\sqrt{\left(p^2 - q^2 + s_0^2\right)^2 + 4p^2q^2} + p^2 - q^2 + s_0^2} + q\sqrt{\sqrt{\left(p^2 - q^2 + s_0^2\right)^2 + 4p^2q^2} - \left(p^2 - q^2 + s_0^2\right)} \right] \frac{1}{\sqrt{2}\sqrt{\left(p^2 - q^2 + s_0^2\right)^2 + 4p^2q^2}} \tag{4}$$

$$\delta_1 = \left[-p\sqrt{\sqrt{\left(p^2 - q^2 + s_0^2\right)^2 + 4p^2q^2} - \left(p^2 - q^2 + s_0^2\right)} + q\sqrt{\sqrt{\left(p^2 - q^2 + s_0^2\right)^2 + 4p^2q^2} + p^2 - q^2 + s_0^2} \right] \frac{1}{\sqrt{2}\sqrt{\left(p^2 - q^2 + s_0^2\right)^2 + 4p^2q^2}} \tag{5}$$

$$\tau_2 = \frac{\sqrt{\sqrt{\left[1 + s_o^2\left(p^2 - q^2\right)\right]^2 + 4s_o^4 p^2 q^2} + 1 + s_o^2\left(p^2 - q^2\right)}}{\sqrt{2}\sqrt{\left[1 + s_o^2\left(p^2 - q^2\right)\right]^2 + 4s_o^4 p^2 q^2}} \tag{6}$$

$$\delta_2 = \frac{\sqrt{\sqrt{\left[1 + s_o^2\left(p^2 - q^2\right)\right]^2 + 4s_o^4 p^2 q^2} - \left[1 + s_o^2\left(p^2 - q^2\right)\right]}}{\sqrt{2}\sqrt{\left[1 + s_o^2\left(p^2 - q^2\right)\right]^2 + 4s_o^4 p^2 q^2}} \tag{7}$$

Substitute τ_1 and δ_1 in the equations for λ and σ given below to determine λ_1 and σ_1 and substitute τ_2 and δ_2 to obtain λ_2 and σ_2:

$$\lambda = \frac{\left[1 + \tau^2 + \delta^2 - \sqrt{\left(1 + \tau^2 + \delta^2\right)^2 - 4\tau^2}\right]\left\{1 + \left(1 - s_o^4\right)\left(\tau^2 + \delta^2\right) - \sqrt{\left[1 + \left(1 - s_o^4\right)\left(\tau^2 + \delta^2\right)\right]^2 - 4\left(1 - s_o^4\right)\tau^2}\right\}}{4\left(1 - s_o^4\right)\tau^2} \tag{8}$$

$$\sigma = \frac{\tau^2 + \delta^2 - \lambda}{\tau^2 + \delta^2 - \lambda - \left[\lambda\left(1 - s_o^4\right)\left(\tau^2 + \delta^2\right) - 1\right]} \tag{9}$$

The elliptic functions $E\left(\sqrt{\sigma}, s_o^2\right)$ and $E\left(\sqrt{1 - \beta^2 m^2}\right)$ in the expression for v (eq. (1)) may be obtained from tables (refs. 8 and 9) or by series expansion.

Supersonic-Leading-Edge Wing

The equation for the sidewash in the region below the right-hand panel of the wing and behind the Mach cone emanating from the wing apex (see appendix A) is

$$v = \frac{V_\infty \alpha}{\pi \sqrt{\beta^2 m^2 - 1}} \left[\tan^{-1} \frac{1 + \beta m \left(\beta \frac{y}{x} \right)}{\sqrt{\beta^2 m^2 - 1}\sqrt{1 - \left(\beta \frac{y}{x} \right)^2 - \left(\beta \frac{z}{x} \right)^2}} \right.$$

$$\left. \tan^{-1} \frac{1 - \beta m \left(\beta \frac{y}{x} \right)}{\sqrt{\beta^2 m^2 - 1}\sqrt{1 - \left(\beta \frac{y}{x} \right)^2 - \left(\beta \frac{z}{x} \right)^2}} \right] \tag{10}$$

In the region behind the plane Mach wave off the wing leading edge and ahead of the Mach cone from the wing apex, the sidewash is given by

$$v = \frac{V_\infty \alpha}{\sqrt{\beta^2 m^2 - 1}} \tag{11}$$

Sonic-Leading-Edge Wing

When the wing leading edge is sonic, the sidewash expressions (eqs. (1) and (10)) simplify to

$$(v)_{\beta m = 1} = \frac{2 V_\infty \alpha \beta \frac{y}{x} \sqrt{1 - \left(\beta \frac{y}{x} \right)^2 - \left(\beta \frac{z}{x} \right)^2}}{\pi \left[1 - \left(\beta \frac{y}{x} \right)^2 \right]} \tag{12}$$

RESULTS AND DISCUSSION

Sidewash Charts

By use of expressions derived herein, the sidewash for all points in the vicinity of infinite-chord triangular wings may be determined. In figures 2 to 7 the variation of the nondimensional sidewash parameter $\frac{v}{V_\infty \alpha}$ with $\beta \frac{y}{x}$ and $\beta \frac{z}{x}$ for βm parameters of 0.4, 0.6, 0.8, 1.0, 1.25, 1.5, 1.75, 2.0, and 2.5 has been presented. Sidewash for βm values falling between those just enumerated may be obtained with sufficient accuracy in most cases by interpolation. In the succeeding discussion of the figures, the nondimensional sidewash $\frac{v}{V_\infty \alpha}$ will be referred to simply as sidewash.

Sidewash Variations With y and z

By assuming β and x to be fixed quantities in the sidewash variations with $\beta \frac{z}{x}$ and $\beta \frac{y}{x}$, it is possible to make a number of observations on the variation of sidewash with vertical and spanwise distances. Another and more vivid method of picturing the flow is to construct contour plots of the sidewash, that is, lines of equal $\frac{v}{V_\infty \alpha}$. For this reason, contour plots have been constructed for βm values of 0.8 and 1.5 and the results are shown in figures 8 and 9.

Subsonic-leading-edge case.- On the surface of the subsonic-leading-edge wing ($z = 0$), the sidewash increases from a zero value at the wing plane of symmetry ($y = 0$) to infinity at the wing leading edge. (See fig. 2.) Outboard of the wing yet in the plane of the wing extended, the sidewash is zero. For a finite value of z, the sidewash increases with y from zero to a maximum, then decreases to zero at the Mach cone from the apex. For a given y value as z is increased (i.e., as z becomes more negative), figures 3 and 8 show that the magnitude of the sidewash decreases except in the region between the wing leading edge and Mach cone where there is an increase to a maximum from the zero value at the plane of the wing extended followed by a decrease.

As the values of the parameter βm (for βm values less than 1) are decreased, the flow field below the wing remains similar in appearance and the magnitude of the sidewash decreases.

Sonic-leading-edge case.- When the wing leading edge is sonic, the sidewash is zero on the Mach cone everywhere except at the point where the wing leading edge and Mach cone coincide. It can be seen in figure 4 that at this point the sidewash is infinite.

Figure 5 presents the variation of sidewash with z for a number of y values and shows that for small values of y the sidewash decreases very slowly with z from its value at $z = 0$ over a large range of z values and drops rapidly near the Mach cone. For the larger values of y, the sidewash decreases more rapidly at the low negative values of z. At a fixed negative value of z, the sidewash increases from zero at the plane of symmetry to a maximum and then drops abruptly to zero at the Mach cone.

Supersonic-leading-edge case.- In order to facilitate the discussion of the supersonic-leading-edge sidewash, a cross section of the wing and Mach cone system is given in the following sketch:
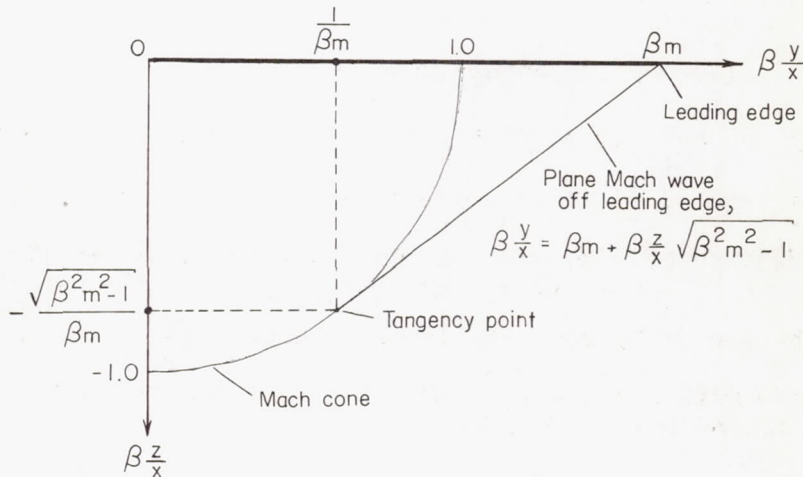
On the Mach cone emanating from the wing apex for the supersonic-leading-edge wing, the sidewash can be considered as having three different values. For that portion of the Mach cone that separates the region behind the Mach cone from the region between the Mach cone and the plane Mach wave off the leading edge, the sidewash has a constant value (eq. (11)). At the point where the plane wave off the leading edge is tangent to the Mach cone from the wing apex, the sidewash has half the constant value given by equation (11). (See figs. 7(d) and 7(e).) Below the tangency point the sidewash has a zero value.

The sidewash on the surface of the wing increases with y from a zero value at the wing plane of symmetry ($y = 0$) to a finite value at the Mach cone from the wing apex. For points on or below the wing outside the Mach cone from the wing apex but within the plane Mach wave off the wing leading edge, the sidewash has a constant value (eq. (11)).

The variation of sidewash with y (see figs. 6 and 9) for a given negative value of z, less than the negative z value of the tangency point, is very similar to the sidewash variation on the wing. For negative values of z greater than that of the tangency point, the sidewash increases gradually with y until it reaches a maximum and then drops abruptly to zero at the Mach cone.

Figures 7 and 9 show that the variation of sidewash with z for a fixed value of y is very slight over a large range of z values. Near the Mach cone, the sidewash drops abruptly to a zero value if the y value is less than that of the plane-wave tangency point and rises abruptly to a constant value if the y-coordinate is greater than that of the tangency point.

Increasing βm (βm values greater than 1) causes a decrease in the maximum values of the sidewash. It is evident that as βm is increased the point of tangency of the leading-edge plane wave moves nearer to the wing symmetry plane and the region between the leading-edge plane wave and the apex Mach cone increases in size relative to the region behind the apex Mach cone.

Sidewash Variations With x

In order that the longitudinal or chordwise variations of sidewash may be conveniently plotted and more easily visualized, the semi-infinite triangular wing has been cut off at a distance x = c from the wing apex. The maximum distance behind the apex of the finite triangular wing that the sidewash can then be represented, by the equations derived herein, is

$$x = c + \beta z$$

or nondimensionally

$$\frac{x}{c} = 1 + \beta m \frac{z}{b/2} \tag{13}$$

where b/2 is the semispan of the finite-chord triangular wing. Beyond the x value of equation (13), the flow field is affected by the finite-wing wake.

The chordwise variation of the sidewash has been plotted in figures 10 and 11 for two values of βm, a subsonic-leading-edge value of 0.8 and a

supersonic-leading-edge value of 1.5; three spanwise locations, $\frac{y}{b/2} = 0.25$,

0.50, and 0.75; and three vertical heights, $\frac{z}{b/2} = -0.1, -0.2,$ and -0.3.

For $\beta m = 0.8$, figure 10 shows that the sidewash rises rapidly to a maximum from its zero value at the Mach cone and then decreases at a much more gradual rate to a finite value at the plane Mach wave off the trailing edge. As previously noted in the discussion of figures 2 and 3, the sidewash magnitudes increase in going from an inboard to an outboard station and decrease (though only slightly over the rear portion of the wing) as the vertical distance is increased.

For the supersonic edge, $\beta m = 1.5$, in figure 11, the most notable feature of the chordwise variations is the abrupt drop in the region immediately behind the Mach cone from the wing apex. In the rearward portions of the wing there is little change of sidewash with vertical height. This is consistent with previous observations. (See figs. 6, 7, and 9.)

CONCLUDING REMARKS

Before an attempt can be made to calculate the aerodynamic forces acting on stores or missiles situated in the immediate vicinity of wings, it is necessary to have a detailed knowledge of the flow field near the wing. The present paper provides some of this needed information by presenting calculations of the lateral flow exterior to lifting, semi-infinite, triangular wings traveling at supersonic speeds. These solutions may also be used directly in determining the sidewash in some regions above and below finite wings. Charts are included from which the sidewash can be obtained, either directly or by interpolation, for all wing sweepback angles and supersonic Mach numbers.

The methods used in deriving the sidewash are based on linearized theory; hence, the results are subject to its limitations.

Langley Aeronautical Laboratory,
    National Advisory Committee for Aeronautics,
        Langley Field, Va., November 6, 1956.

APPENDIX A

DETERMINATION OF SIDEWASH EXPRESSIONS

The purpose of this appendix is to give the derivation of the side-wash equations. The derivations presented are carried out for $\beta = 1$ so that the sidewash and associated formulas given in subsequent sections are dependent only on m, y/x, and z/x. By use of the Prandtl-Glauert rule, which demonstrates that the flow-field velocities at any Mach number must depend on βm, $\beta \frac{y}{x}$, and $\beta \frac{z}{x}$, the sidewash expressions may be rewritten to apply for all Mach numbers. (See eqs. (1), (10), (11), and (12) in the main body of this paper.)

Subsonic-Leading-Edge Case

In reference 4, H. J. Stewart gives the following differential equation (with a change in notation) for the complex sidewash velocity:

$$\frac{dV}{d\zeta} = \frac{-i2V_\infty \alpha s_o^3}{mE\left(\sqrt{1 - m^2}\right)} \frac{(1 + \zeta^2)(1 - \zeta^2)}{\left[\left(\zeta^2 + s_o^2\right)\left(\zeta^2 s_o^2 + 1\right)\right]^{3/2}} \tag{A1}$$

where

$$s_o = \frac{1 - \sqrt{1 - m^2}}{m}$$

and

$$\zeta = p + iq = \frac{\frac{z}{x} + i\frac{y}{x}}{1 + \sqrt{1 - \left(\frac{y}{x}\right)^2 - \left(\frac{z}{x}\right)^2}} \tag{A2}$$

Integration of equation (A1) leads to

$$V = v + i\bar{v}$$

$$= \frac{-izV_{\infty}\alpha s_0}{m\left(1 - s_0^4\right)E\left(\sqrt{1 - m^2}\right)}\left[E\left(\xi, \sqrt{1 - s_0^4}\right) - \right.$$

$$\left. F\left(\xi, \sqrt{1 - s_0^4}\right) + E\left(\eta, \sqrt{1 - s_0^4}\right) - F\left(\eta, \sqrt{1 - s_0^4}\right)\right] + C \qquad (A3)$$

The complex variables ξ and η originate through variable changes necessary in the integration of equation (A1) and their relation to ζ is given by

$$\xi = \frac{\zeta}{\sqrt{\zeta^2 + s_0^2}}$$

$$\eta = \frac{1}{\sqrt{1 + s_0^2\zeta^2}}$$

It is convenient to designate the real and imaginary parts of these new variables by τ_1, δ_1, τ_2, and δ_2 so that

$$\xi = \tau_1 + i\delta_1$$

and

$$\eta = \tau_2 - i\delta_2$$

$\left(\tau_1,\ \delta_1,\ \tau_2,\ \text{and}\ \delta_2\right.$ in terms of y/x and z/x are given in the text by eqs. (2), (3), (4), (5), (6), and (7)$\left.\right)$. The constant C in equation (A3) is determined by the condition that the sidewash (real part of eq. (A3)) must be zero on the Mach cone.

Of interest here is the real part of equation (A3), that is, the side-wash. Thus, the problem remaining is to find the imaginary parts of the elliptic integrals E and F in equation (A3). With

$$F\left(\tau \pm i\delta, \sqrt{1 - s_o^4}\right) = F_r \pm iF_i$$

and

$$E\left(\tau \pm i\delta, \sqrt{1 - s_o^4}\right) = E_r \pm iE_i$$

the equation for the sidewash may be written

$$v = \frac{2V_\infty \alpha s_o}{m\left(1 - s_o^4\right)E\left(\sqrt{1 - m^2}\right)}\left[\left(E_i\right)_1 - \left(F_i\right)_1 - \left(E_i\right)_2 + \left(F_i\right)_2\right] + C$$

$$(A4)$$

Reference 3 gives

$$F_i = F\left(\sqrt{\sigma}, s_o^2\right)$$

Thus

$$\left(F_i\right)_1 = F\left(\sqrt{\sigma_1}, s_o^2\right) \tag{A5}$$

and

$$\left(F_i\right)_2 = F\left(\sqrt{\sigma_2}, s_o^2\right) \tag{A6}$$

In appendix B the imaginary part of the elliptic integral E with complex argument has been derived and yields

$$\left(E_i\right)_1 = -E\left(\sqrt{\sigma_1}, s_o^2\right) + F\left(\sqrt{\sigma_1}, s_o^2\right) +$$

$$\frac{\left[1 - \left(1 - s_o^4\right)\lambda_1\right]\sqrt{\sigma_1}\sqrt{1 - \sigma_1}\sqrt{1 - s_o^4\sigma_1}}{1 - \left[1 - \left(1 - s_o^4\right)\lambda_1\right]\sigma_1} \tag{A7}$$

and

$$\left(E_i\right)_2 = -E\left(\sqrt{\sigma_2}, s_o^2\right) + F\left(\sqrt{\sigma_2}, s_o^2\right) +$$

$$\frac{\left[1 - \left(1 - s_o^4\right)\lambda_2\right]\sqrt{\sigma_2}\sqrt{1 - \sigma_2}\sqrt{1 - s_o^4\sigma_2}}{1 - \left[1 - \left(1 - s_o^4\right)\lambda_2\right]\sigma_2} \tag{A8}$$

By substituting equations (A5), (A6), (A7), and (A8) into equation (A4), the sidewash is found to be

$$v = \frac{2V_\infty \alpha s_o}{m\left(1 - s_o^4\right)E\left(\sqrt{1 - m^2}\right)}\left\{-E\left(\sqrt{\sigma_1}, s_o^2\right) + \right.$$

$$\frac{\left[1 - \left(1 - s_o^4\right)\lambda_1\right]\sqrt{\sigma_1}\sqrt{1 - \sigma_1}\sqrt{1 - s_o^4\sigma_1}}{1 - \left[1 - \left(1 - s_o^4\right)\lambda_1\right]\sigma_1} + E\left(\sqrt{\sigma_2}, s_o^2\right) -$$

$$\left. \frac{\left[1 - \left(1 - s_o^4\right)\lambda_2\right]\sqrt{\sigma_2}\sqrt{1 - \sigma_2}\sqrt{1 - s_o^4\sigma_2}}{1 - \left[1 - \left(1 - s_o^4\right)\lambda_2\right]\sigma_2} \right\} \tag{A9}$$

In order to obtain the equation for v that is presented in the text,
m (in the denominator of (eq. (A9)) has been replaced as follows by its
equivalent in terms of s_O:

$$m = \frac{2s_O}{1 + s_O^2}$$

Also, it has been found that the boundary conditions are satisfied with
the constant of integration set equal to zero.

Supersonic-Leading-Edge Case

It has been demonstrated in reference 2 that the flow field exterior
to a lifting or nonlifting semi-infinite triangular wing with supersonic
leading edges is the sum of the flow fields of two lines of pressure
sources coincident with the wing leading edges. Directly obtained in
reference 2 by virtue of this result is the longitudinal perturbation
velocity u for points in the flow field. The u velocity below the
lifting wing and behind the Mach cone from the wing apex is given by the
following equation:

$$u = \frac{-V_\infty \alpha m}{\pi \sqrt{m^2 - 1}} \left[\cos^{-1} \frac{x - my}{\sqrt{(y - mx)^2 - z^2(m^2 - 1)}} + \right.$$

$$\left. \cos^{-1} \frac{x + my}{\sqrt{(y + mx)^2 - z^2(m^2 - 1)}} \right] \tag{A10}$$

and for points between the Mach cone and the plane wave off the leading
edge is given by

$$u = \frac{-V_\infty \alpha m}{\sqrt{m^2 - 1}} \tag{A11}$$

It should be noted that the positive square roots are to be taken in the
denominator of the arc cosine terms of equation (A10) in conjunction with
the principal values of the arc cosines. Equations for the vertical per-
turbation velocity or downwash have been derived in reference 3. In the
remainder of this section the lateral perturbation velocity, referred to
herein as sidewash, will be obtained by the procedure used in reference 3.

By considering the relationship between the perturbation-velocity potential and the streamwise velocity component,

$$\frac{\partial \phi}{\partial x} = u$$

expressions giving the perturbation-velocity potential ϕ and lateral velocity component v may be written

$$\phi = \int_{x_0}^{x} u(x',y,z)dx' \tag{A12}$$

$$v = \frac{\partial \phi}{\partial y} = \frac{\partial}{\partial y} \int_{x_0}^{x} u(x',y,z)dx' \tag{A13}$$

The integration in equations (A12) and (A13) is along a line parallel to the x-axis from a point x_0, where the potential ϕ and velocity u are zero, to a point in the region where the velocity potential or sidewash is desired.

Two possible paths of integration are shown in figure 12 for points behind the apex Mach cone. One path intersects both the plane wave and Mach cone whereas the other intersects only the Mach cone. Mathematically, it can be shown that the first of these integration paths corresponds to the condition that $x < my$ and the second, to the condition that $x > my$. Consider the first of the two paths of integration. The velocity potential at a point x from equations (A10), (A11), and (A12) is given as follows:

$$\phi = -\frac{V_\infty \alpha m}{\sqrt{m^2-1}} \left[\int_{\frac{y}{m} - \frac{z\sqrt{m^2-1}}{m}}^{\sqrt{y^2+z^2}} dx' + \frac{1}{\pi} \int_{\sqrt{y^2+z^2}}^{x} \cos^{-1} \frac{x' - my}{\sqrt{(y-mx')^2 - z^2(m^2-1)}} dx' + \right.$$

$$\left. \frac{1}{\pi} \int_{\sqrt{y^2+z^2}}^{x} \cos^{-1} \frac{x' + my}{\sqrt{(y+mx')^2 - z^2(m^2-1)}} dx' \right] \tag{A14}$$

Performing the first two integrations and then differentiating with respect to y gives rise to

$$v = -\frac{V_\infty \alpha m}{\pi} \left\{ \frac{y}{\sqrt{y^2 + z^2}} - \frac{\pi}{m\sqrt{m^2 - 1}} - \frac{y}{\sqrt{y^2 + z^2}} + \right.$$

$$\int_{\sqrt{y^2+z^2}}^{x} \frac{mx'^2 - x'y - mz^2}{\sqrt{x'^2 - y^2 - z^2}\left[(y - mx')^2 - z^2(m^2 - 1)\right]} \, dx' -$$

$$\left. \int_{\sqrt{y^2+z^2}}^{x} \frac{mx'^2 + x'y - mz^2}{\sqrt{x'^2 - y^2 - z^2}\left[(y + mx')^2 - z^2(m^2 - 1)\right]} \, dx' \right\} \qquad (A15)$$

The first two terms in equation (A15) are obtained from the first integral of equation (A14). The third and fourth terms result from differentiating the first arc cosine integral in equation (A14) and the last term in equation (A15) comes from differentiating the second arc cosine term of equation (A14). Note that the first and third terms of equation (A15) cancel. The first integral in equation (A15) when evaluated (remember when substituting the lower limits that $x < my$) gives

$$\frac{1}{m\sqrt{m^2 - 1}} \left(\tan^{-1} \frac{x - my}{\sqrt{m^2 - 1}\sqrt{x^2 - y^2 - z^2}} + \sqrt{m^2 - 1} \cosh^{-1} \frac{x}{\sqrt{y^2 + z^2}} + \frac{\pi}{2} \right)$$

$$(A16)$$

The evaluation of the second integral in equation (A15) may be obtained from the evaluation of the first integral in equation (A15) (expression (A16)) by replacing y by $-y$ and changing the sign before the $\frac{\pi}{2}$ term. This procedure yields

$$-\frac{1}{m\sqrt{m^2 - 1}} \left(\tan^{-1} \frac{x + my}{\sqrt{m^2 - 1}\sqrt{x^2 - y^2 - z^2}} + \sqrt{m^2 - 1} \cosh^{-1} \frac{x}{\sqrt{y^2 + z^2}} - \frac{\pi}{2} \right)$$

$$(A17)$$

When expressions (A16) and (A17) are substituted for the integrals in equation (A15), the sidewash behind the apex Mach cone for the case where $x < my$ is seen to be

$$v = -\frac{V_\infty \alpha}{\pi \sqrt{m^2 - 1}}\left(\tan^{-1}\frac{x - my}{\sqrt{m^2 - 1}\sqrt{x^2 - y^2 - z^2}} - \tan^{-1}\frac{x + my}{\sqrt{m^2 - 1}\sqrt{x^2 - y^2 - z^2}}\right)$$

(A18)

When the path of integration to the point x intersects only the Mach cone, the sidewash from equations (A10) and (A13) may be written as

$$v = -\frac{V_\infty \alpha m}{\pi \sqrt{m^2 - 1}}\frac{\partial}{\partial y}\left\{\int_{\sqrt{y^2+z^2}}^{x}\cos^{-1}\left[\frac{x_1 - my}{\sqrt{(y - mx_1)^2 - z^2(m^2 - 1)}}\right]dx' + \right.$$

$$\left.\int_{\sqrt{y^2+z^2}}^{x}\cos^{-1}\left[\frac{x_1 + my}{\sqrt{(y + mx_1)^2 - z^2(m^2 - 1)}}\right]dx'\right\}$$

(A19)

Carrying out the differentiation in equation (A19) yields

$$v = -\frac{V_\infty \alpha m}{\pi}\left\{\int_{\sqrt{y^2+z^2}}^{x}\frac{mx'^2 - x'y - mz^2}{\sqrt{x'^2 - y^2 - z^2}\left[(y - mx')^2 - z^2(m^2 - 1)\right]}dx' - \right.$$

$$\left.\int_{\sqrt{y^2+z^2}}^{x}\frac{mx'^2 - x'y - mz^2}{\sqrt{x'^2 - y^2 - z^2}\left[(y + mx')^2 - z^2(m^2 - 1)\right]}dx'\right\}$$

which when integrated with $x > my$ results in the following equation:

$$v = - \frac{V_\infty \alpha}{\pi \sqrt{m^2 - 1}} \left(\tan^{-1} \frac{x - my}{\sqrt{m^2 - 1} \sqrt{x^2 - y^2 - z^2}} + \sqrt{m^2 - 1} \cosh^{-1} \frac{x}{\sqrt{y^2 + z^2}} \right.$$

$$\left. \tan^{-1} \frac{x + my}{\sqrt{m^2 - 1} \sqrt{x^2 - y^2 - z^2}} - \sqrt{m^2 - 1} \cosh^{-1} \frac{x}{\sqrt{y^2 + z^2}} \right)$$

$$= - \frac{V_\infty \alpha}{\pi \sqrt{m^2 - 1}} \left(\tan^{-1} \frac{x - my}{\sqrt{m^2 - 1} \sqrt{x^2 - y^2 - z^2}} - \tan^{-1} \frac{x + my}{\sqrt{m^2 - 1} \sqrt{x^2 - y^2 - z^2}} \right)$$

$$(A20)$$

It can be seen from equations (A18) and (A20) that the sidewash behind the Mach cone is given for all points by the same expression.

The sidewash in the region between the plane Mach wave off the leading edge and the Mach cone below the right wing panel is given by

$$v = - \frac{V_\infty \alpha m}{\sqrt{m^2 - 1}} \frac{\partial}{\partial y} \int_{\frac{y}{m} - \frac{z\sqrt{m^2 - 1}}{m}}^{x} dx'$$

which, when the indicated operations are performed, becomes

$$v = \frac{V_\infty \alpha}{\sqrt{m^2 - 1}} \qquad\qquad (A21)$$

Sonic-Leading-Edge Case

The sonic-leading-edge sidewash is most simply obtained from equation (A20). Setting m equal to 1 in equation (A20) gives rise to an indeterminancy which may easily be evaluated to yield the required sidewash

$$v = \frac{2V_\infty \alpha \frac{y}{x} \sqrt{1 - \left(\frac{y}{x}\right)^2 - \left(\frac{z}{x}\right)^2}}{\pi \left[1 - \left(\frac{y}{x}\right)^2\right]} \tag{A22}$$

APPENDIX B

EVALUATION OF IMAGINARY PART OF AN INCOMPLETE ELLIPTIC

INTEGRAL OF THE SECOND KIND WITH A COMPLEX ARGUMENT

In reference 3 the real part of the incomplete elliptic integral $E(\tau+i\delta,k)$ and the real and imaginary parts of the elliptic integral $F(\tau+i\delta,k)$ have been derived. The purpose of this appendix is to obtain the imaginary part of the elliptic integral $E(\tau\pm i\delta,k)$ which is necessary in determining the sidewash. (See eq. (A4).)

The incomplete elliptic integral of the second kind with a complex argument may be written as

$$E(\tau\pm i\delta,k) = \int_0^{\tau\pm i\delta} \frac{\sqrt{1 - k^2\xi^2}}{\sqrt{1 - \xi^2}}\, d\xi \tag{B1}$$

where

$$k = \sqrt{1 - s_o^4}$$

When the Jacobian transformation

$$\tau \pm i\delta = \xi = sn(\mu,k) = sn(\mu_r\pm\mu_i,k) \tag{B2}$$

is introduced, equation (B1) becomes

$$E(\tau\pm i\delta,k) = \int_0^{F_r\pm iF_i} dn^2(\mu,k)d\mu \tag{B3}$$

Evaluation of the real and imaginary parts of the upper limit of equation (B3), that is,

$$F_r \pm iF_i = \int_0^{\tau\pm i\delta} \frac{d\xi}{\sqrt{1 - \xi^2}\,\sqrt{1 - k^2\xi^2}}$$

is given in reference 3. (See also eqs. (A5) and (A6).)

As pointed out in reference 3, the integration in equation (B3) is most conveniently performed in two steps: first, along the real axis to F_r, and then parallel to the imaginary axis from F_r to $F_r \pm iF_i$. Thus, equation (B3) becomes

$$E(\tau \pm i\delta, k) = \int_0^{F_r} dn^2(\mu_r, k)d\mu_r \pm i \int_0^{F_i} dn^2(F_r \pm i\mu_i, k)d\mu_i \qquad (B4)$$

The first integral in equation (B4) is real and may be excluded from further consideration. It is convenient in determining the imaginary part of the second term to expand the delta-amplitude elliptic function with the aid of the following formula given in reference 8, page 24:

$$dn(F_r \pm i\mu_i, k) = \frac{dn(F_r, k)cn(\mu_i, k')dn(\mu_i, k')}{1 - sn^2(\mu_i, k')dn^2(F_r, k)} \mp \frac{ik^2 sn(F_r, k)cn(F_r, k)sn(\mu_i, k')}{1 - sn^2(\mu_i, k')dn^2(F_r, k)}$$

With the use of the relationship in the second integral of equation (B4), the imaginary part of $E(\tau \pm i\delta, k)$ is given by

$$I.P.\left[E(\tau \pm i\delta, k)\right] = \pm \int_0^{F_i} \left\{ \frac{dn^2(F_r, k)cn^2(\mu_i, k')dn^2(\mu_i, k')}{\left[1 - sn^2(\mu_i, k')dn^2(F_r, k)\right]^2} - \right.$$

$$\left. \frac{k^4 sn^2(F_r, k)cn^2(F_r, k)sn^2(\mu_i, k')}{\left[1 - sn^2(\mu_i, k')dn^2(F_r, k)\right]^2} \right\} d\mu_i \qquad (B5)$$

By use of the integration formulas given on pages 218 and 219 of reference 8, the imaginary part of $E(\tau \pm i\delta, k)$ in terms of Jacobian elliptic functions becomes

$$I.P.\left[E(\tau \pm i\delta, k)\right] = \pm \left[F_i(sn\ F_i, k') - E(sn\ F_i, k') + \right.$$

$$\left. \frac{dn^2(F_r, k)sn(F_i, k')cn(F_i, k')dn(F_i, k')}{1 - dn^2(F_r, k)sn^2(F_i, k')} \right] \qquad (B6)$$

From the change in variable of equation (B2), that is,

$$\tau \pm i\delta = sn(F_r \pm F_i, k)$$

and by defining λ and σ as follows:

$$\lambda = sn^2(F_r, k) \tag{B7}$$

$$\sigma = sn^2(F_i, k') \tag{B8}$$

reference 3 has shown that τ and δ may be related to λ and σ by

$$\tau^2 = \frac{\lambda(1 - k'^2\sigma)}{(1 - \sigma + k^2\lambda\sigma)^2} \tag{B9}$$

$$\delta^2 = \frac{\sigma(1 - \sigma)(1 - \lambda)(1 - k^2\lambda)}{(1 - \sigma + k^2\lambda\sigma)^2} \tag{B10}$$

and

$$\lambda = \frac{\left[1 + \tau^2 + \delta^2 - \sqrt{(1 + \tau^2 + \delta^2)^2 - 4\tau^2}\right]\left\{1 + k^2(\tau^2 + \delta^2) - \sqrt{\left[1 + k^2(\tau^2 + \delta^2)\right]^2 - 4k^2\tau^2}\right\}}{4k^2\tau^2} \tag{B11}$$

$$\sigma = \frac{\tau^2 + \delta^2 - \lambda}{\tau^2 + \delta^2 - \lambda - \left[\lambda k^2(\tau^2 + \delta^2) - 1\right]} \tag{B12}$$

Other useful relationships which may be formed by use of equations (B7) and (B8) are

$$cn(F_r, k) = \sqrt{1 - \lambda} \tag{B13}$$

$$dn(F_r, k) = \sqrt{1 - k^2\lambda} \tag{B14}$$

$$cn(F_i,k') = \sqrt{1 - \sigma} \tag{B15}$$

$$dn(F_i,k') = \sqrt{1 - k'^2\sigma} \tag{B16}$$

By use of the relationships given in equations (B7), (B8), (B13), (B14), (B15), and (B16), the imaginary part of the elliptic function $E(\tau \pm i\delta,k)$, defined by equation (B6), can now be written in terms of λ, σ, and k as

$$I.P.\left[E(\tau \pm i\delta,k)\right] = \pm \left[F\left(\sqrt{\sigma},k'\right) - E\left(\sqrt{\sigma},k'\right) + \frac{(1 - k^2\lambda)\sqrt{\sigma}\sqrt{1 - \sigma}\sqrt{1 - k'^2\sigma}}{1 - (1 - k^2\lambda)\sigma}\right]$$

In equations (A6) and (A7), k and k' have been replaced by their equivalents $\sqrt{1 - s_o^4}$ and s_o^2.

REFERENCES

1. Alford, William J., Jr.: Theoretical and Experimental Investigation of the Subsonic-Flow Fields Beneath Swept and Unswept Wings With Tables of Vortex-Induced Velocities. NACA TN 3738, 1956.

2. Jones, Robert T.: Thin Oblique Airfoils at Supersonic Speed. NACA Rep. 851, 1946. (Supersedes NACA TN 1107.)

3. Nielsen, Jack N., and Perkins, Edward W.: Charts for the Conical Part of the Downwash Field of Swept Wings at Supersonic Speeds. NACA TN 1780, 1948.

4. Stewart, H. J.: The Lift of a Delta Wing at Supersonic Speeds. Quarterly Appl. Math., vol. IV, no. 3, Oct. 1946, pp. 246-254.

5. Lagerstrom, P. A., Graham, Martha E., and Grosslight, G.: Downwash and Sidewash Induced by Three-Dimensional Lifting Wings in Supersonic Flow. Rep. No. SM-13007, Douglas Aircraft Co., Inc., Apr. 14, 1947.

6. Lomax, Harvard, and Heaslet, Max. A.: A Special Method for Finding Body Distortions That Reduce the Wave Drag of Wing and Body Combinations at Supersonic Speeds. NACA RM A55B16, 1955.

7. Nielsen, Jack N., and Pitts, William C.: General Theory of Wave-Drag Reduction for Combinations Employing Quasi-Cylindrical Bodies With an Application to Swept-Wing and Body Combinations. NACA TN 3722, 1956. (Supersedes NACA RM A55B07.)

8. Byrd, Paul F., and Friedman, Morris D.: Handbook of Elliptic Integrals for Engineers and Physicists. Lange, Maxwell & Springer Ltd. (New York), 1954.

9. Jahnke, Eugene, and Emde, Fritz: Tables of Functions. Fourth ed., Dover Publications, 1945.
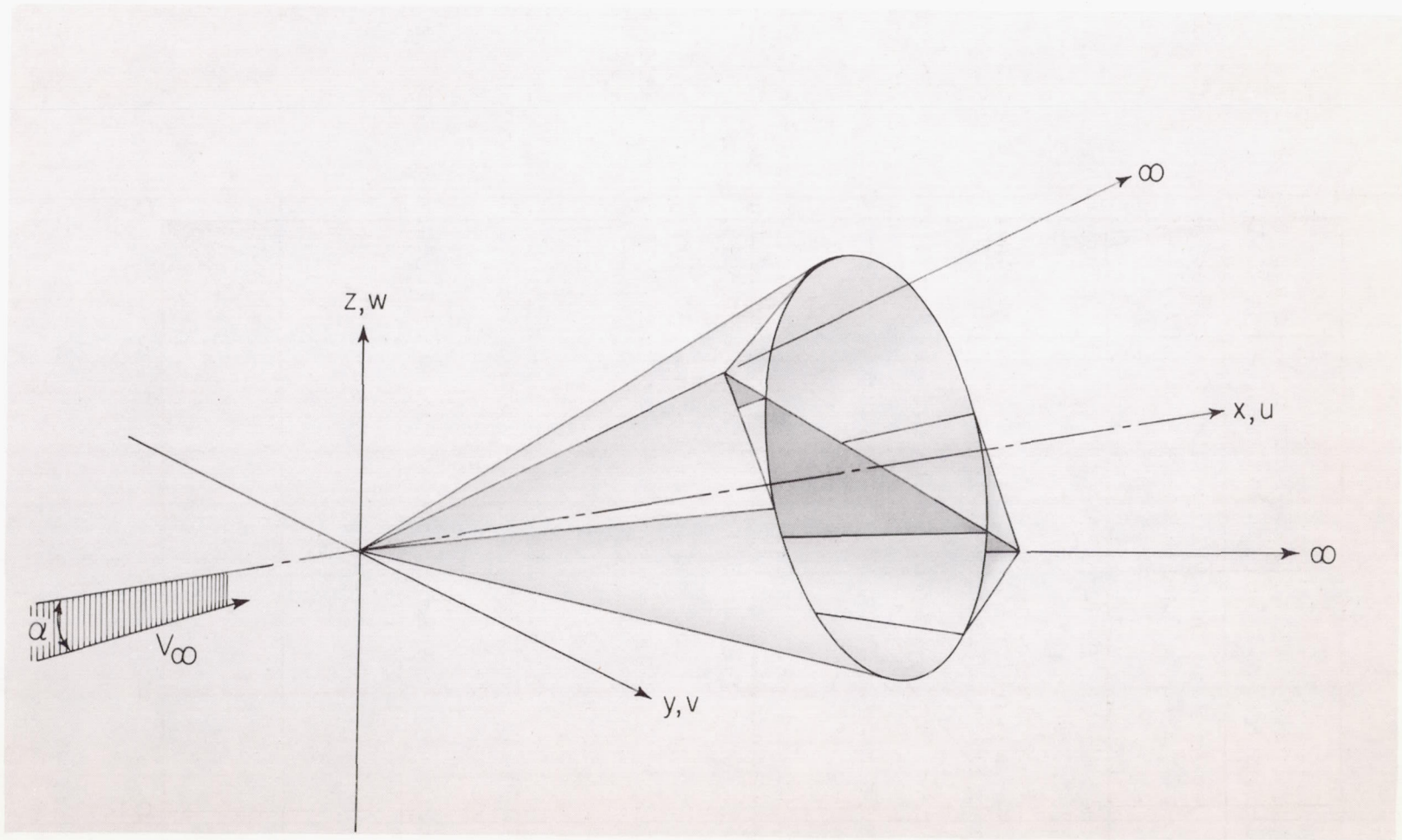
Figure 1.- Sketch of supersonic-leading-edge wing showing system of axes used in analysis and the positive directions of the flow velocities and angle of attack.
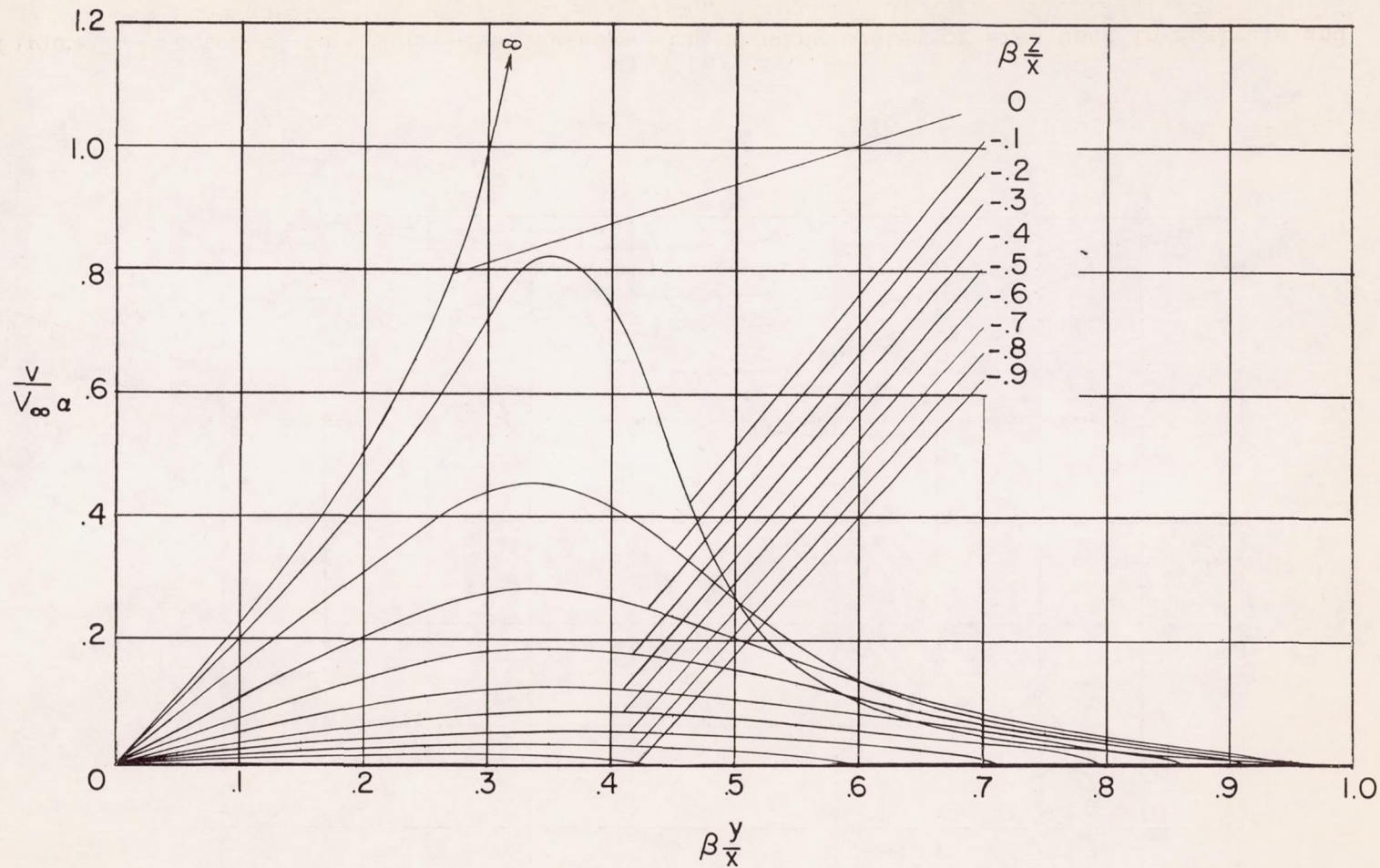
(a) βm = 0.4.

Figure 2.- Variation of the subsonic-leading-edge sidewash with $\beta\frac{y}{x}$ for a range of $\beta\frac{z}{x}$ and βm values.
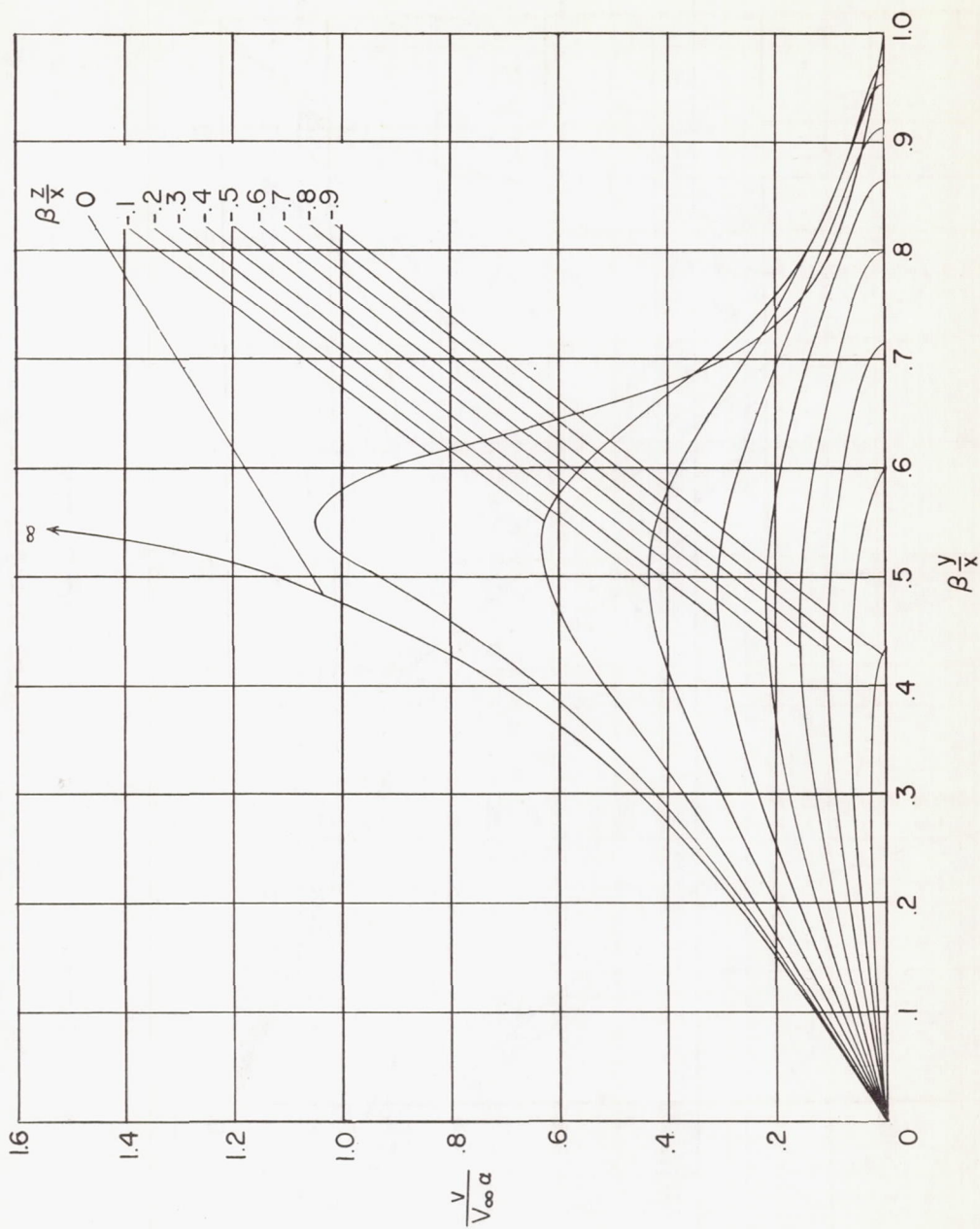
(b) $\beta m = 0.6$.

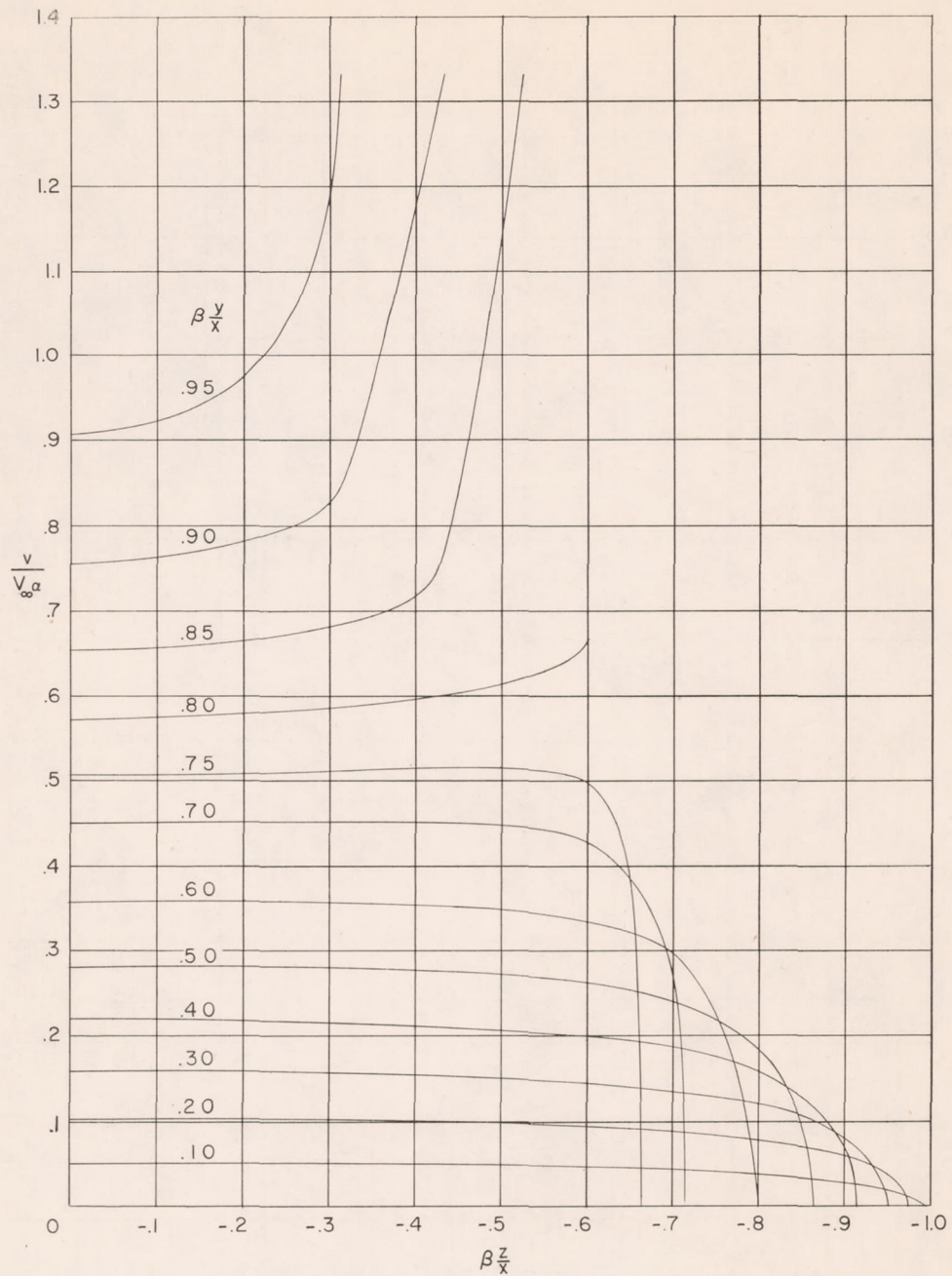Figure 2.- Continued.
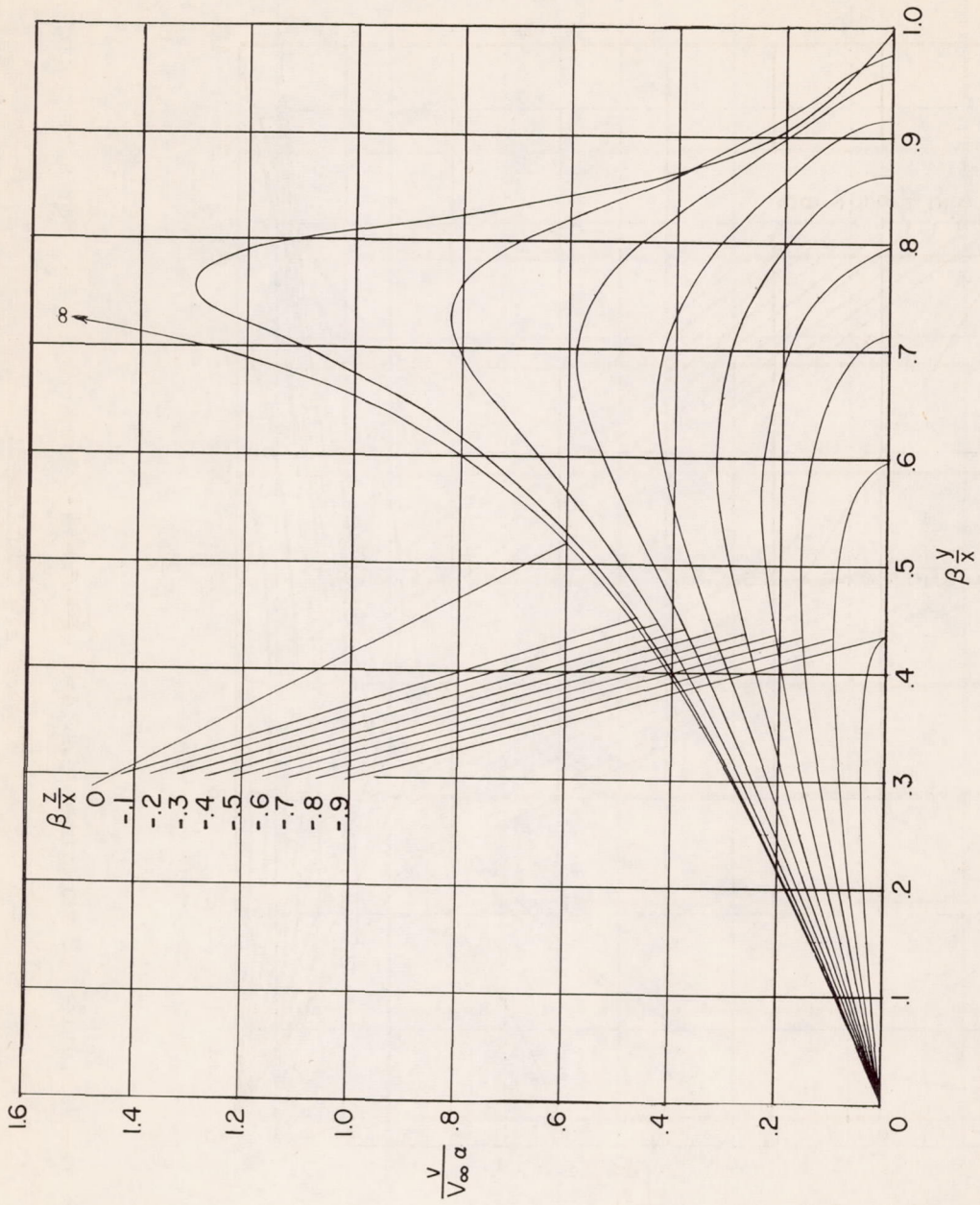
(c) $\beta m = 0.8$.

Figure 2.- Concluded.
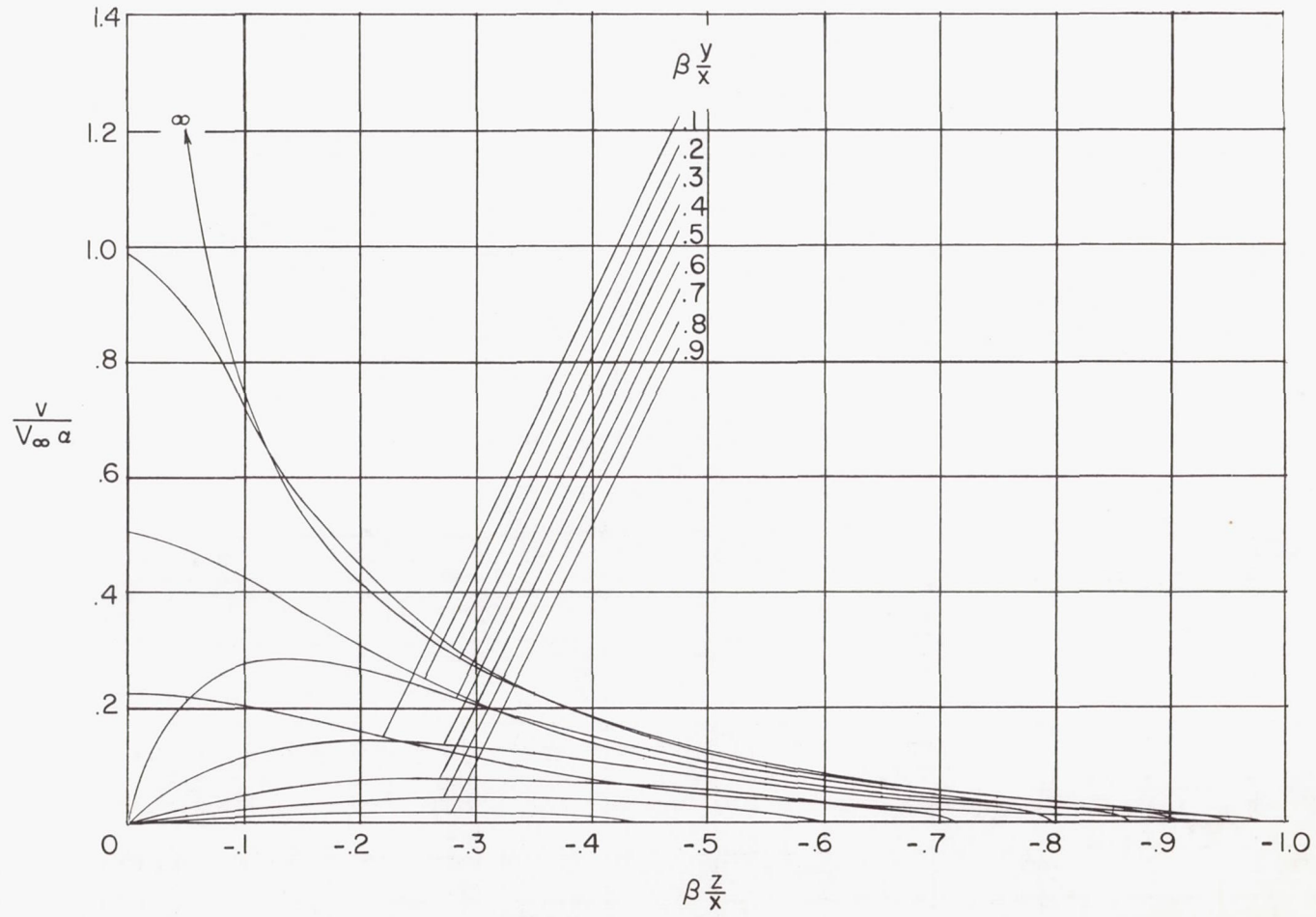
(a) $\beta m = 0.4.$

Figure 3.- Variation of the subsonic-leading-edge sidewash with $\beta\frac{z}{x}$ for a range of $\beta\frac{y}{x}$ and βm values.
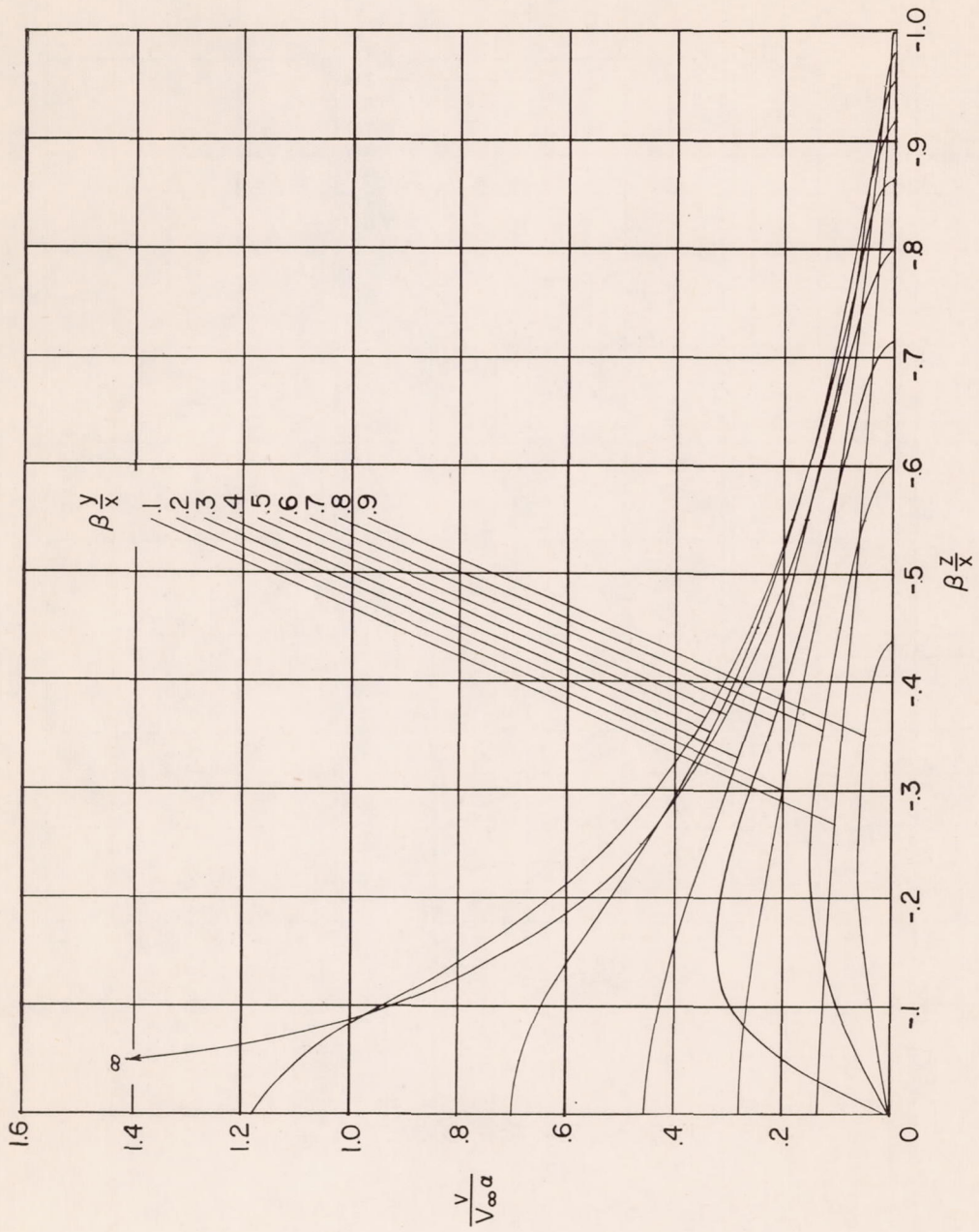
(b) βm = 0.6.

Figure 3.- Continued.
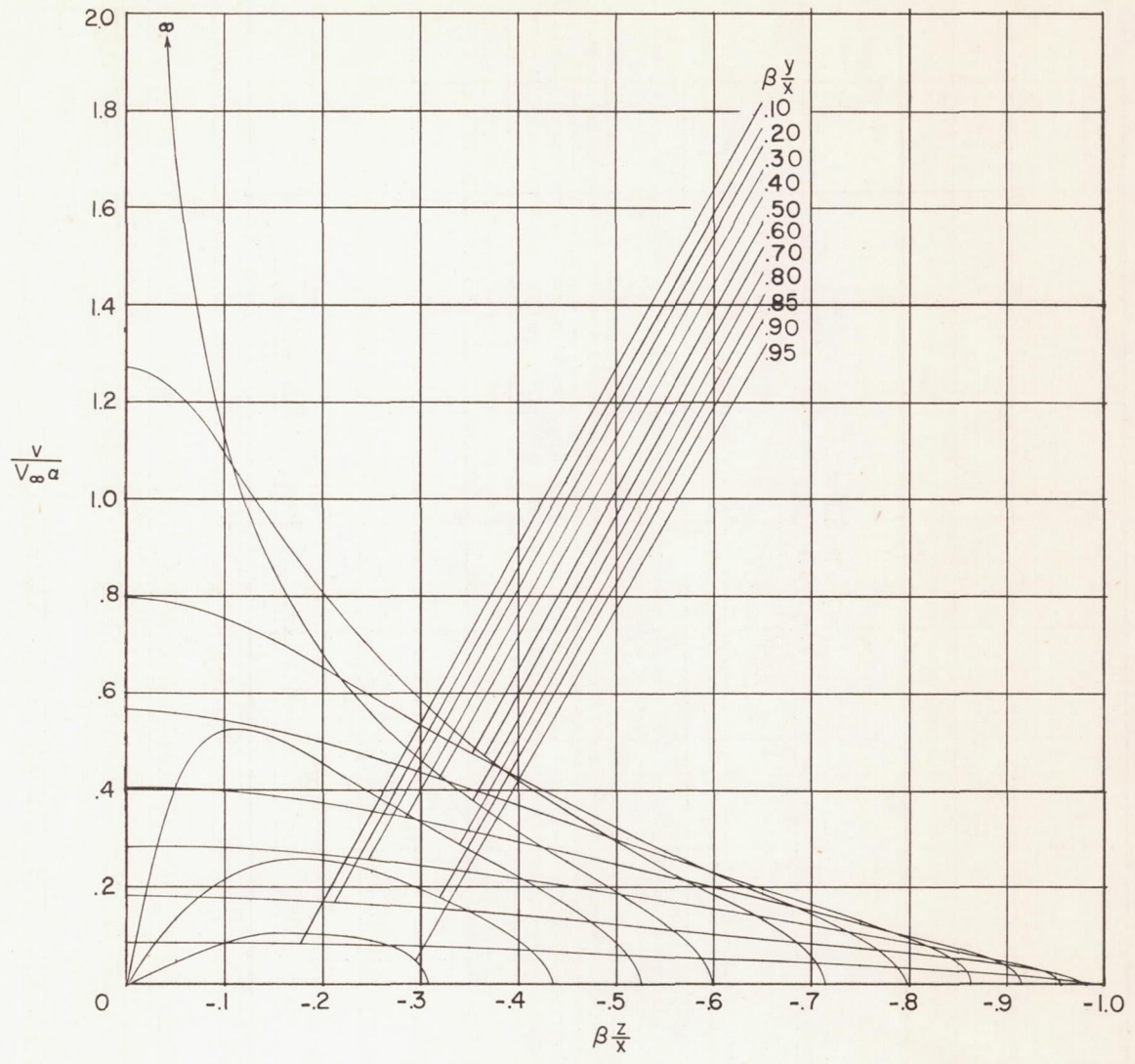
(c) $\beta m = 0.8$.

Figure 3.- Concluded.
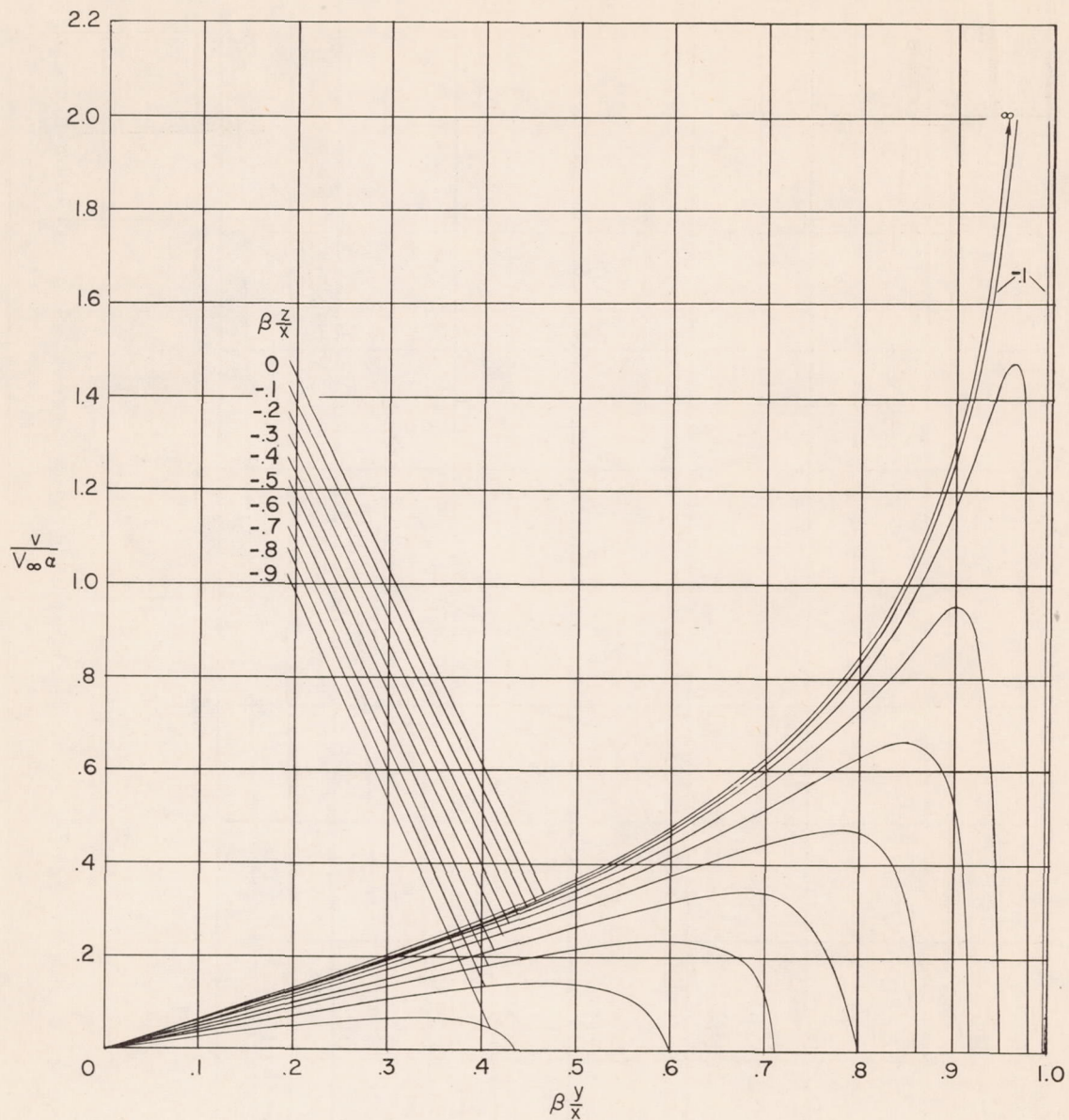
Figure 4.- Variation of the sonic-leading-edge ($\beta m = 1$) sidewash with $\beta\frac{y}{x}$ for a range of $\beta\frac{z}{x}$ values.
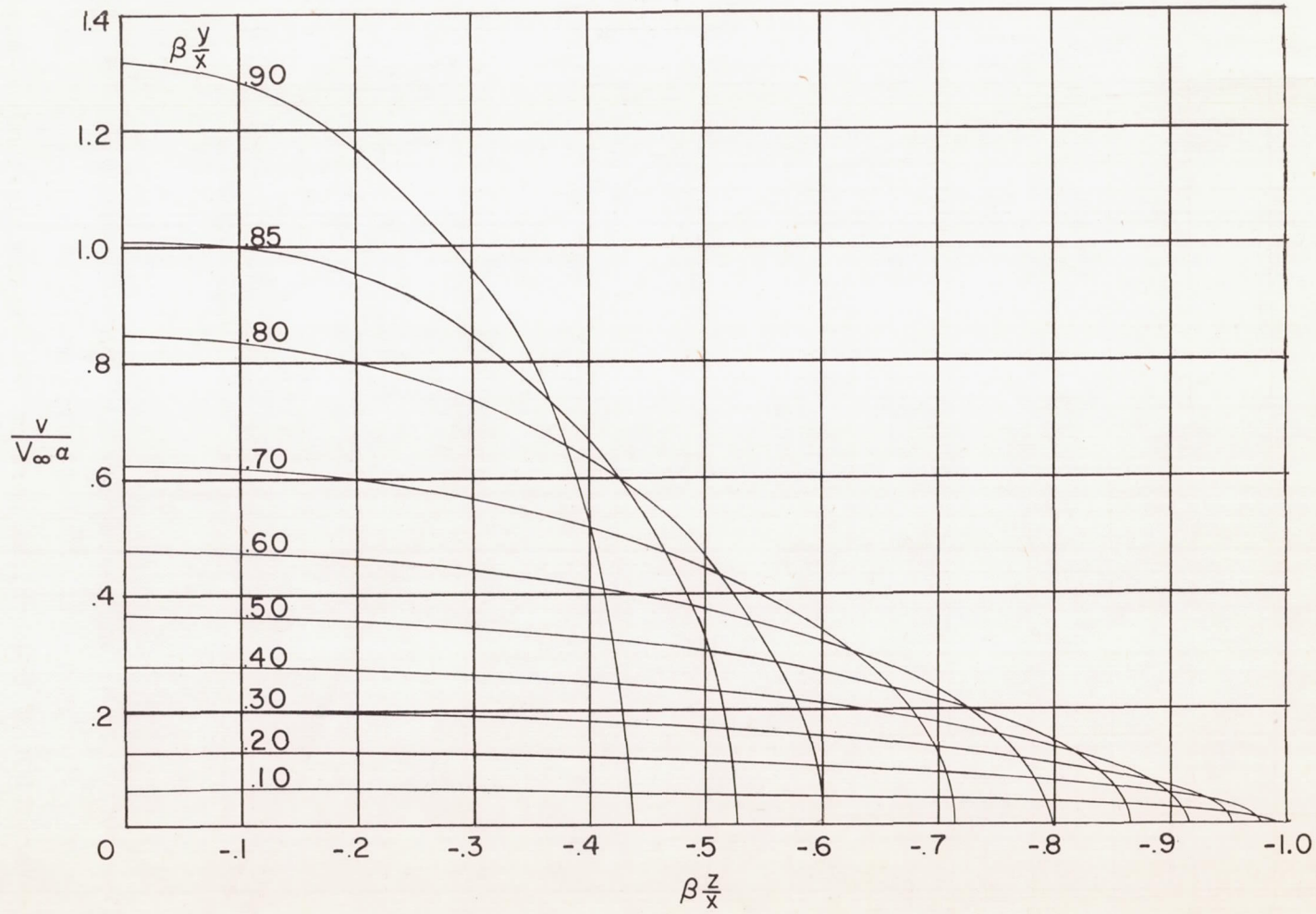
Figure 5.- Variation of the sonic-leading-edge ($\beta m = 1$) sidewash with $\beta\frac{z}{x}$ for a range of $\beta\frac{y}{x}$ values.
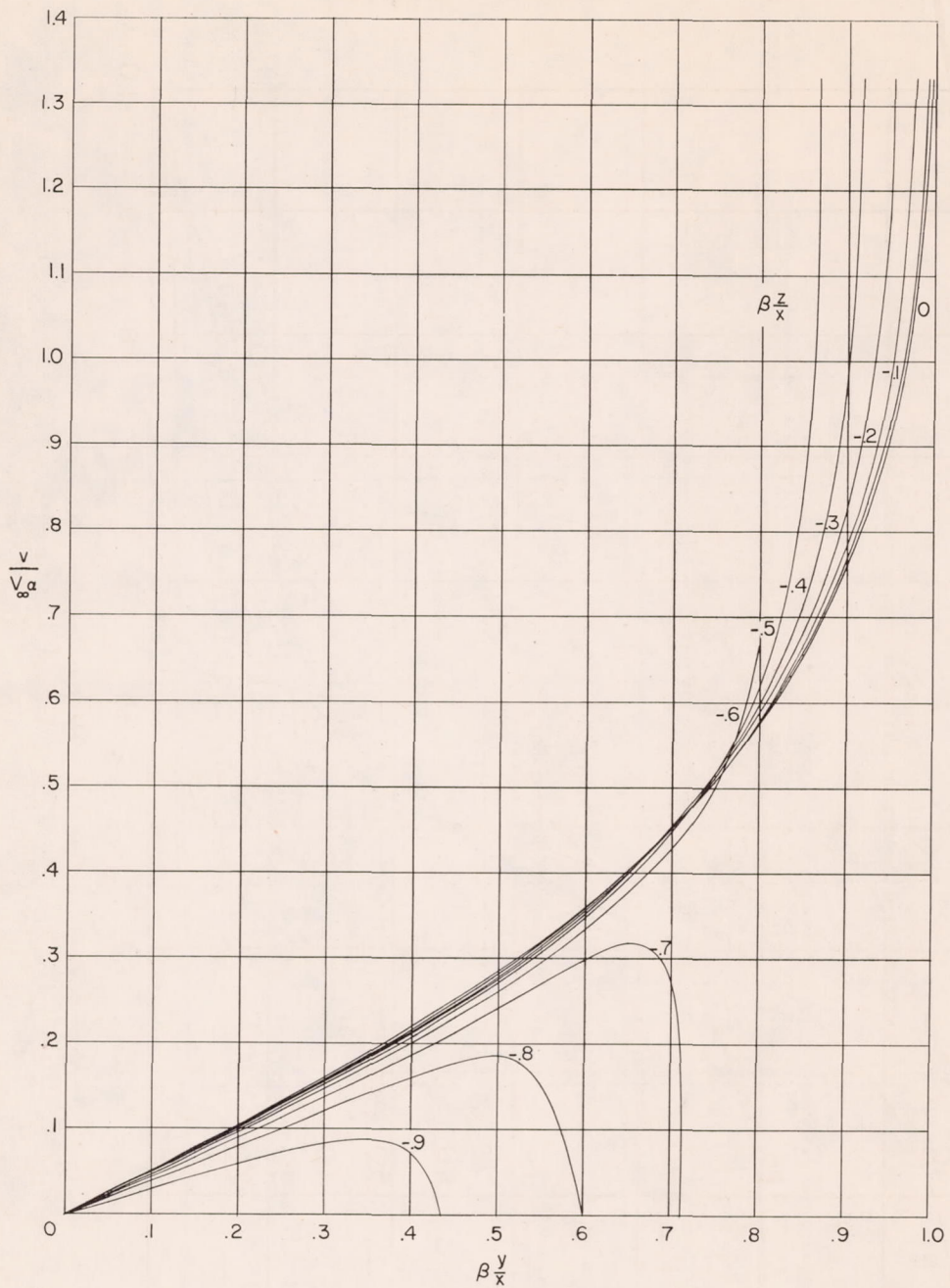
(a) $\beta m = 1.25$.

Figure 6.- Variation of the conical part of the supersonic-leading-edge sidewash with $\beta \frac{y}{x}$ for a range of $\beta \frac{z}{x}$ and βm values.
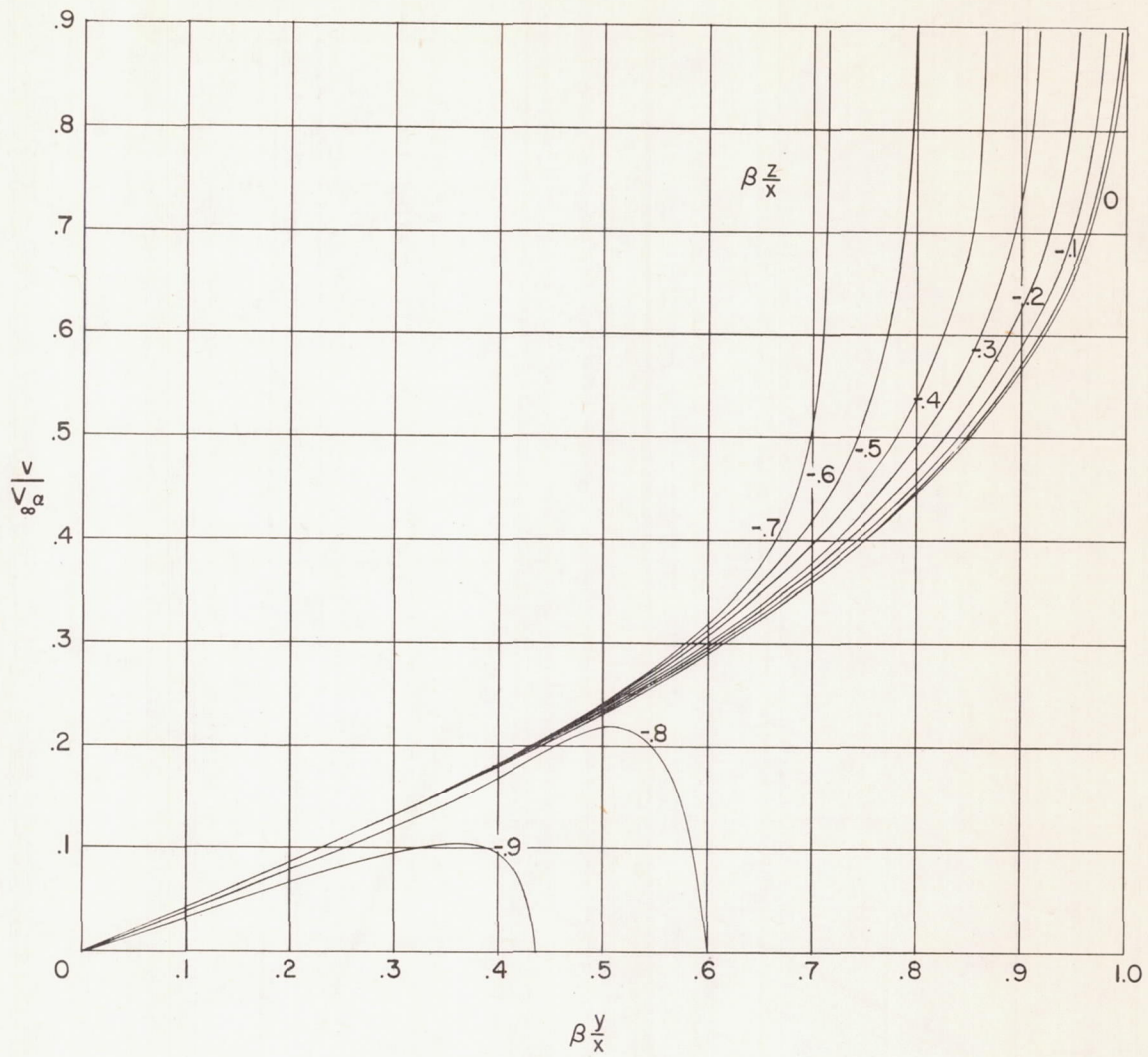
(b) $\beta m = 1.5$.

Figure 6.- Continued.
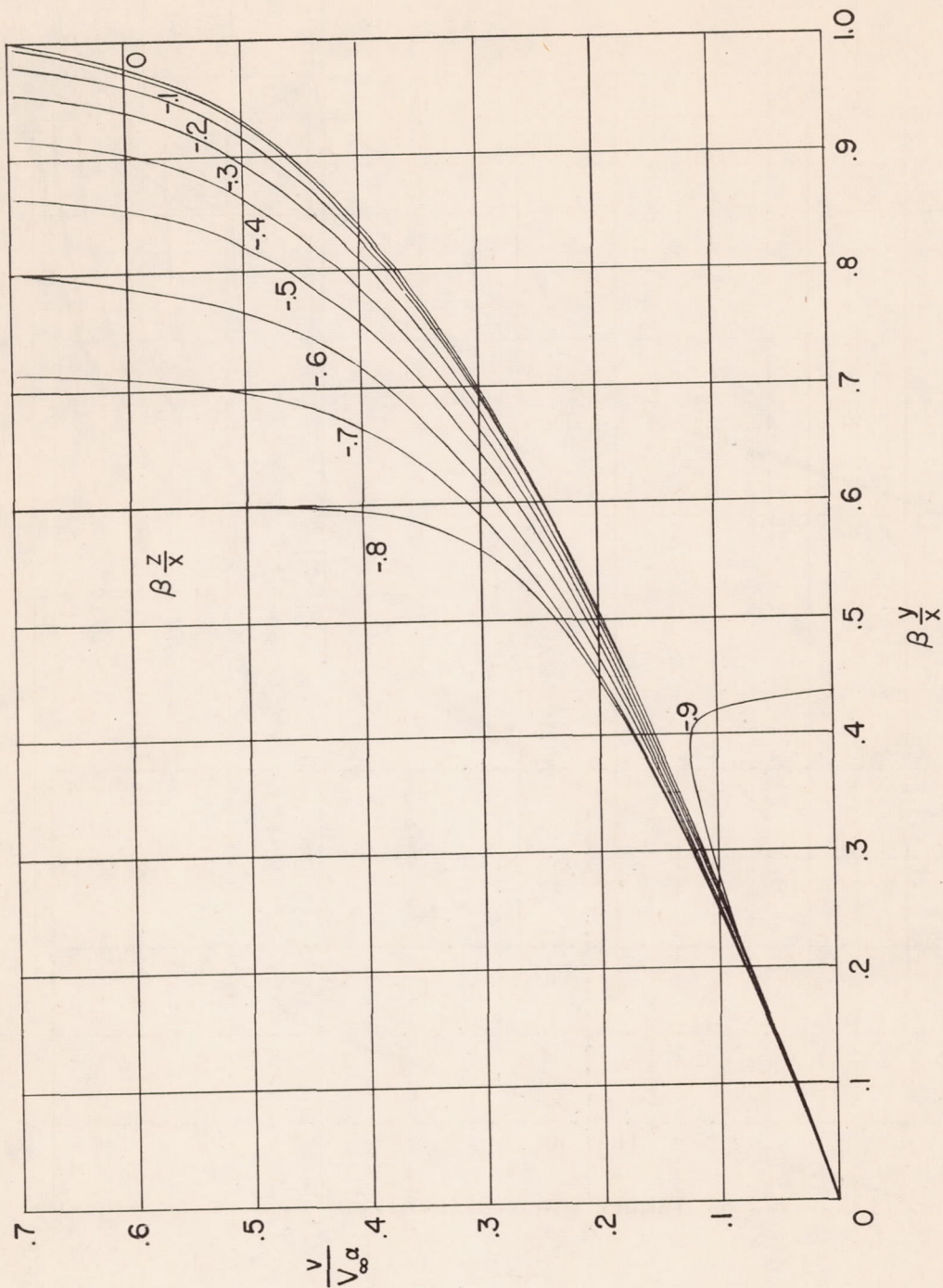
(c) $\beta m = 1.75$.

Figure 6.- Continued.

(d)   βm = 2.0.
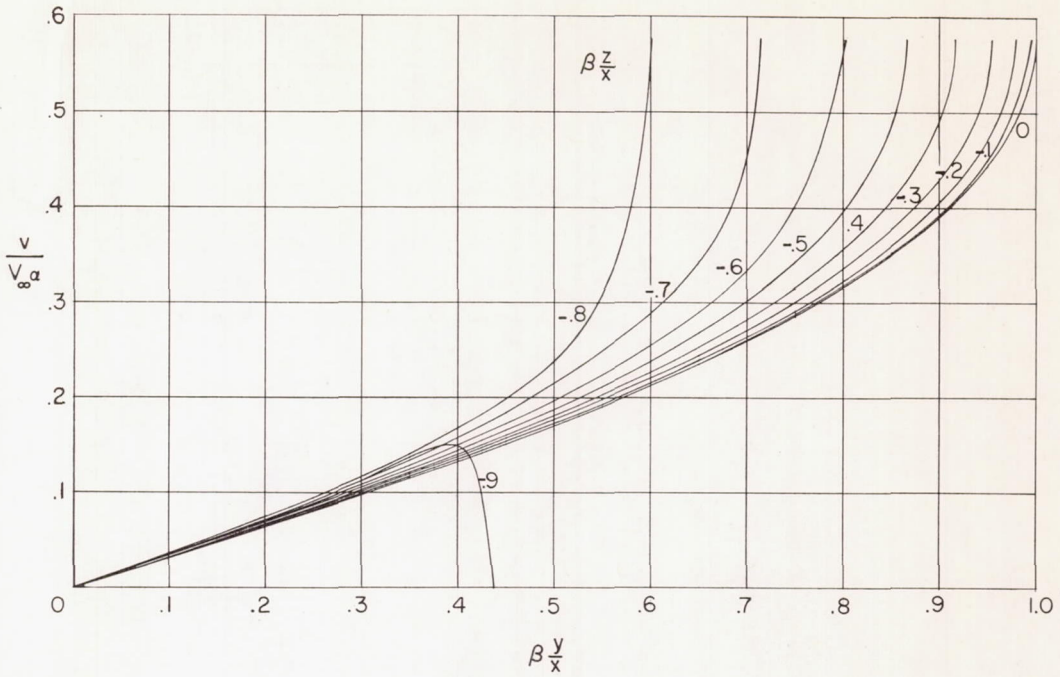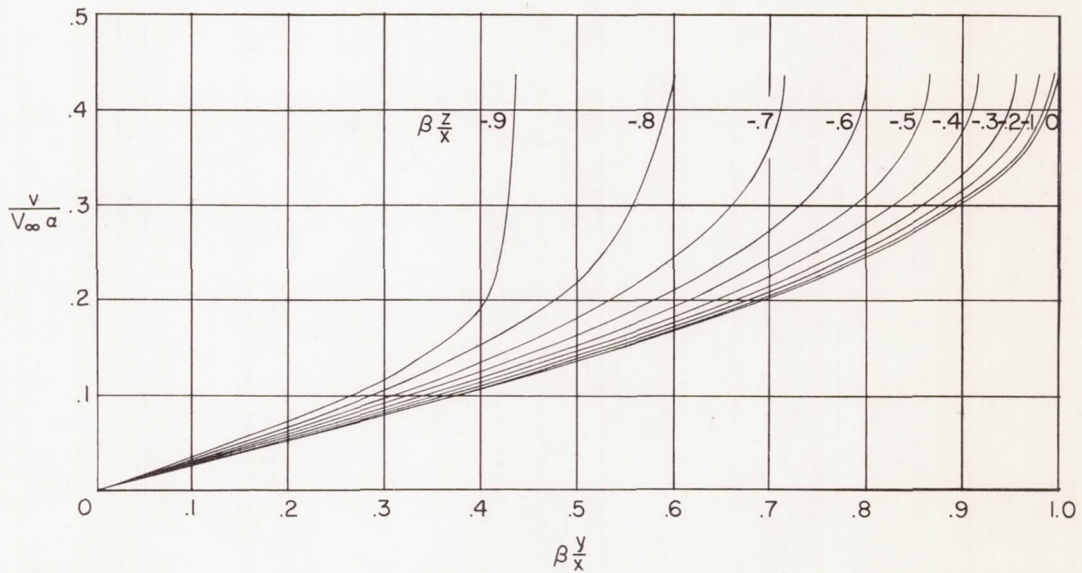
(e)   βm = 2.5.

Figure 6.- Concluded.

(a) $\beta m = 1.25$.

Figure 7.- Variation of the conical part of the supersonic-leading-edge

sidewash with $\beta\frac{z}{x}$ for a range of $\beta\frac{y}{x}$ and βm values.
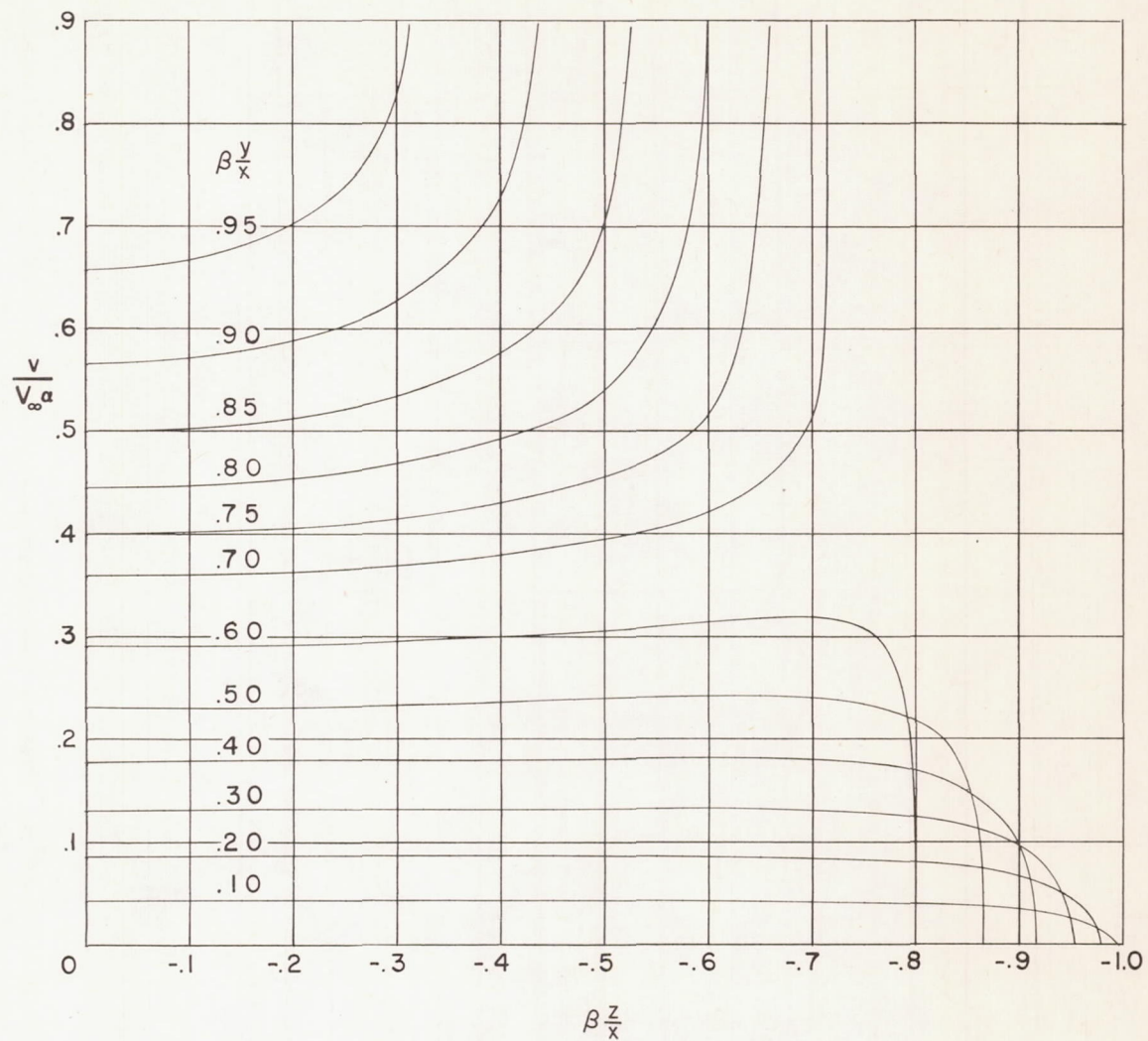
(b) βm = 1.5.

Figure 7.- Continued.
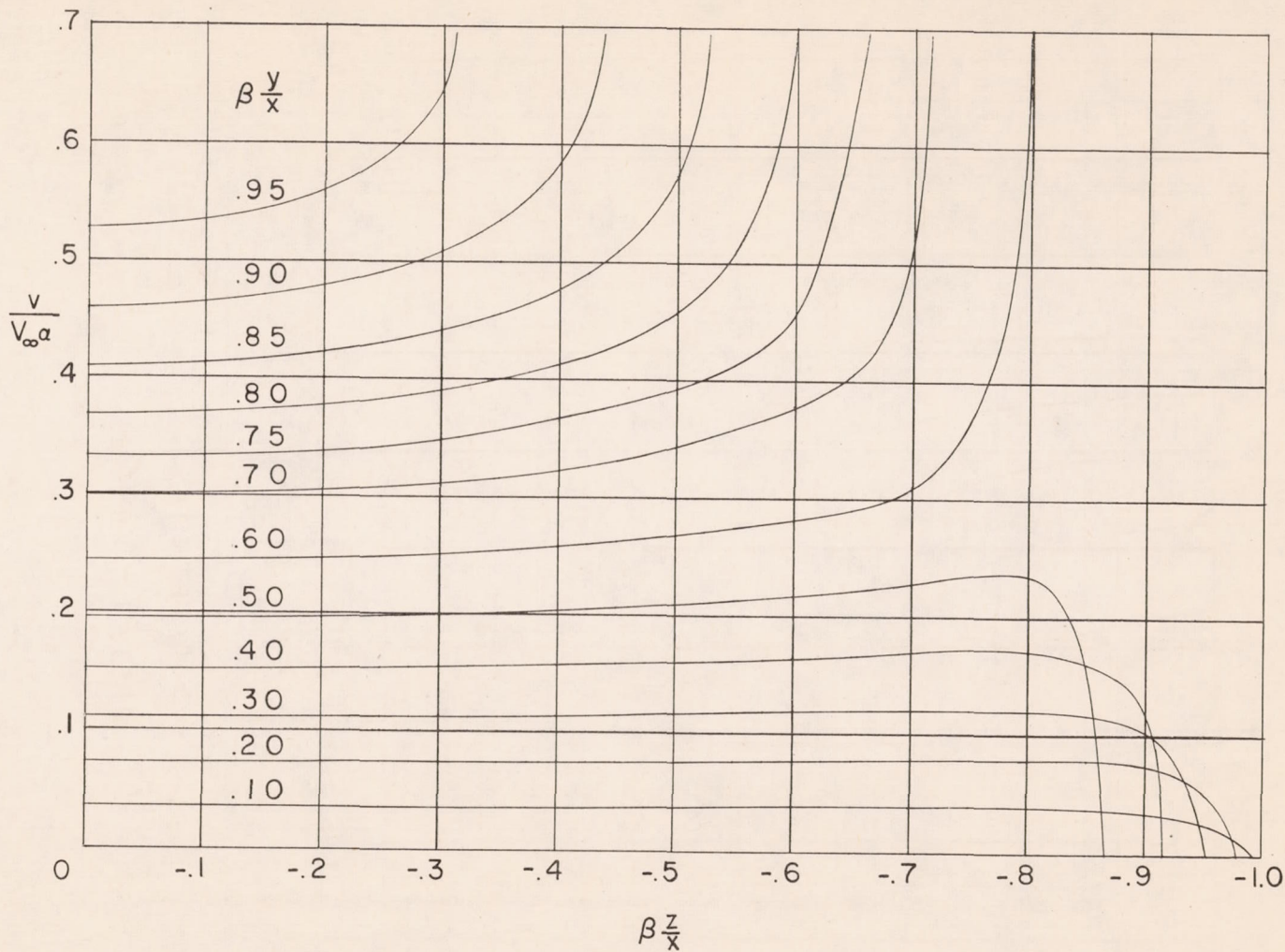
(c) $\beta m = 1.75$.

Figure 7.- Continued.
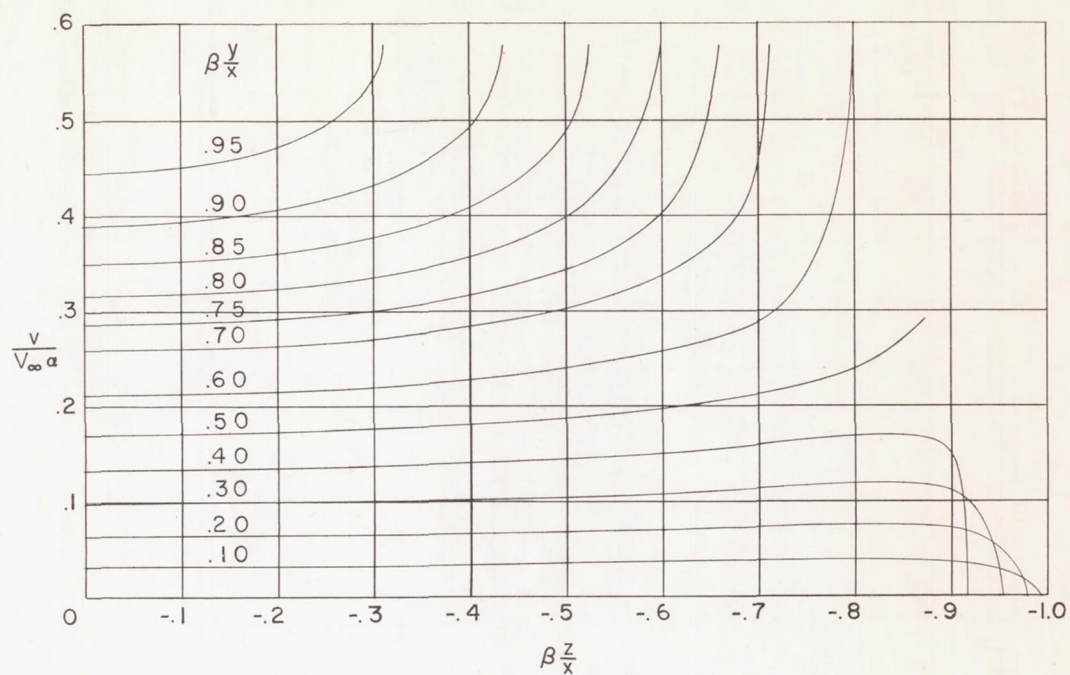
(d) $\beta m = 2.0$.
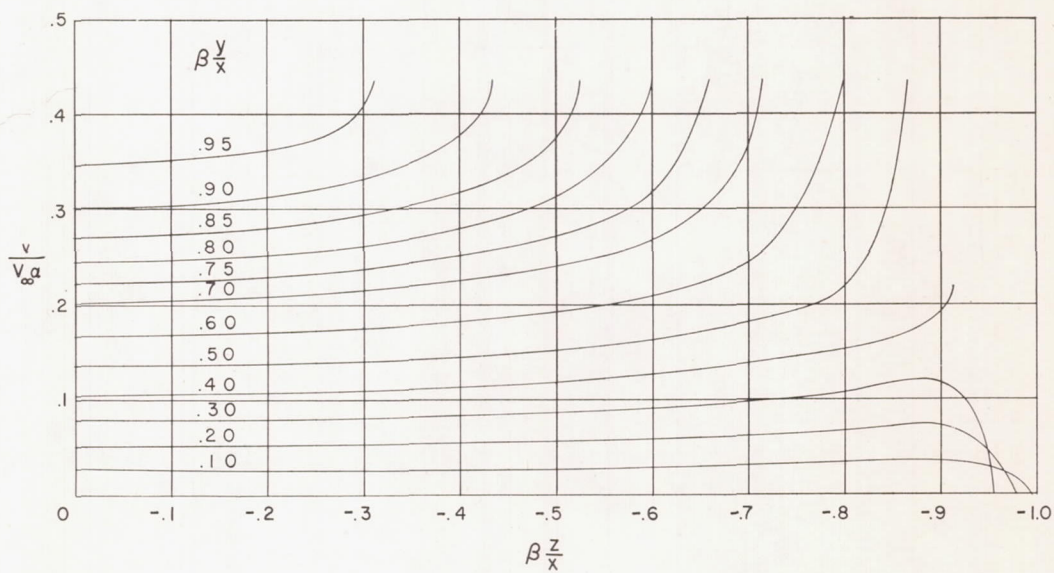
(e) $\beta m = 2.5$.

Figure 7.- Concluded.
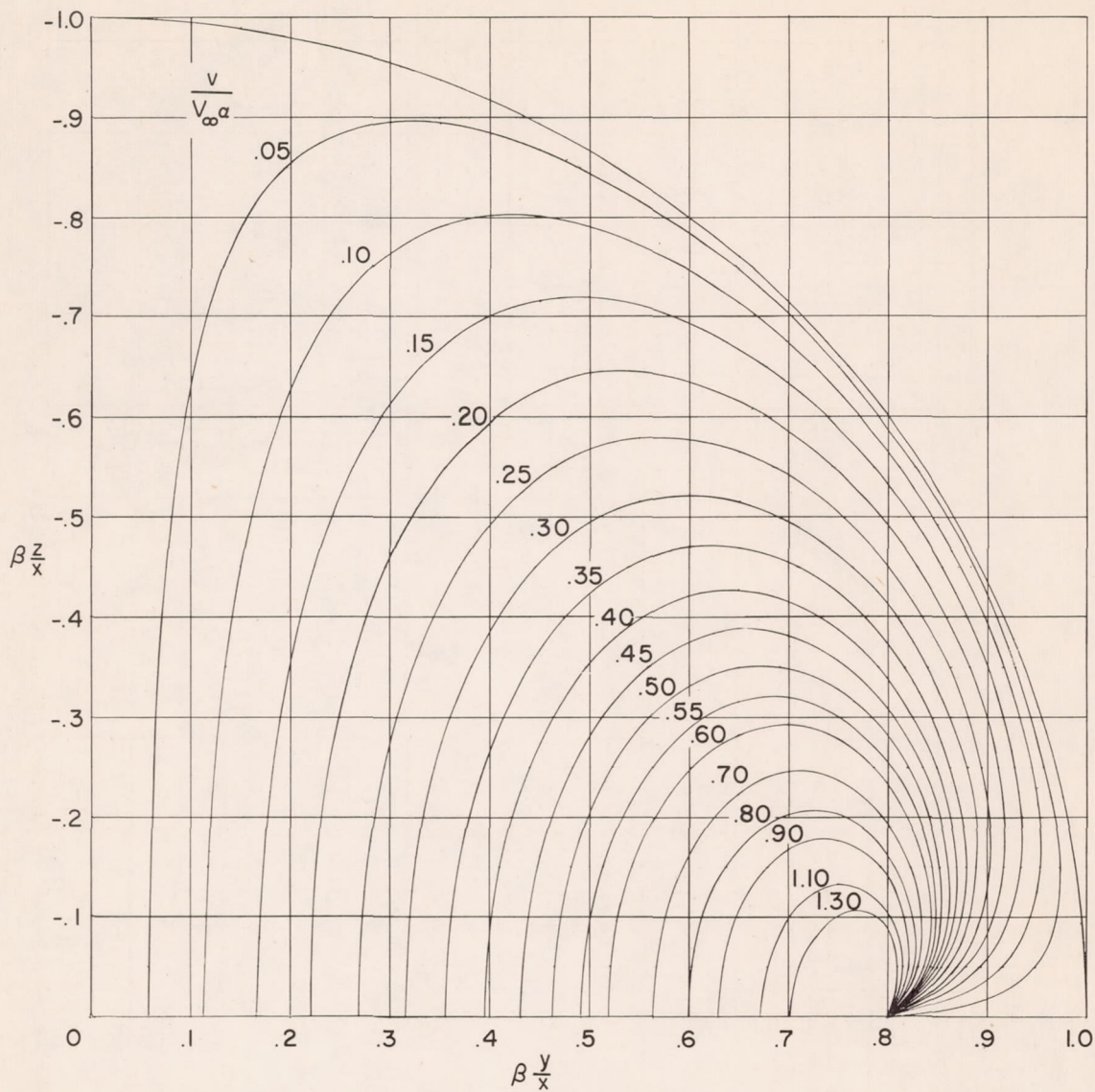
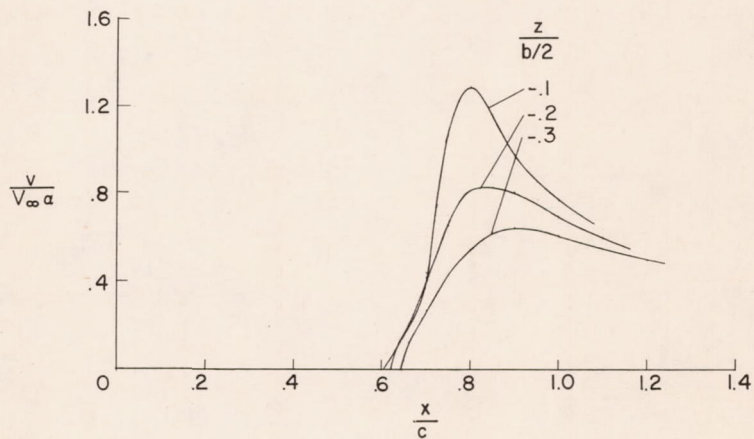Figure 8.- Sidewash contours for a subsonic-leading-edge lifting triangular wing of infinite chord. $\beta m = 0.8$.
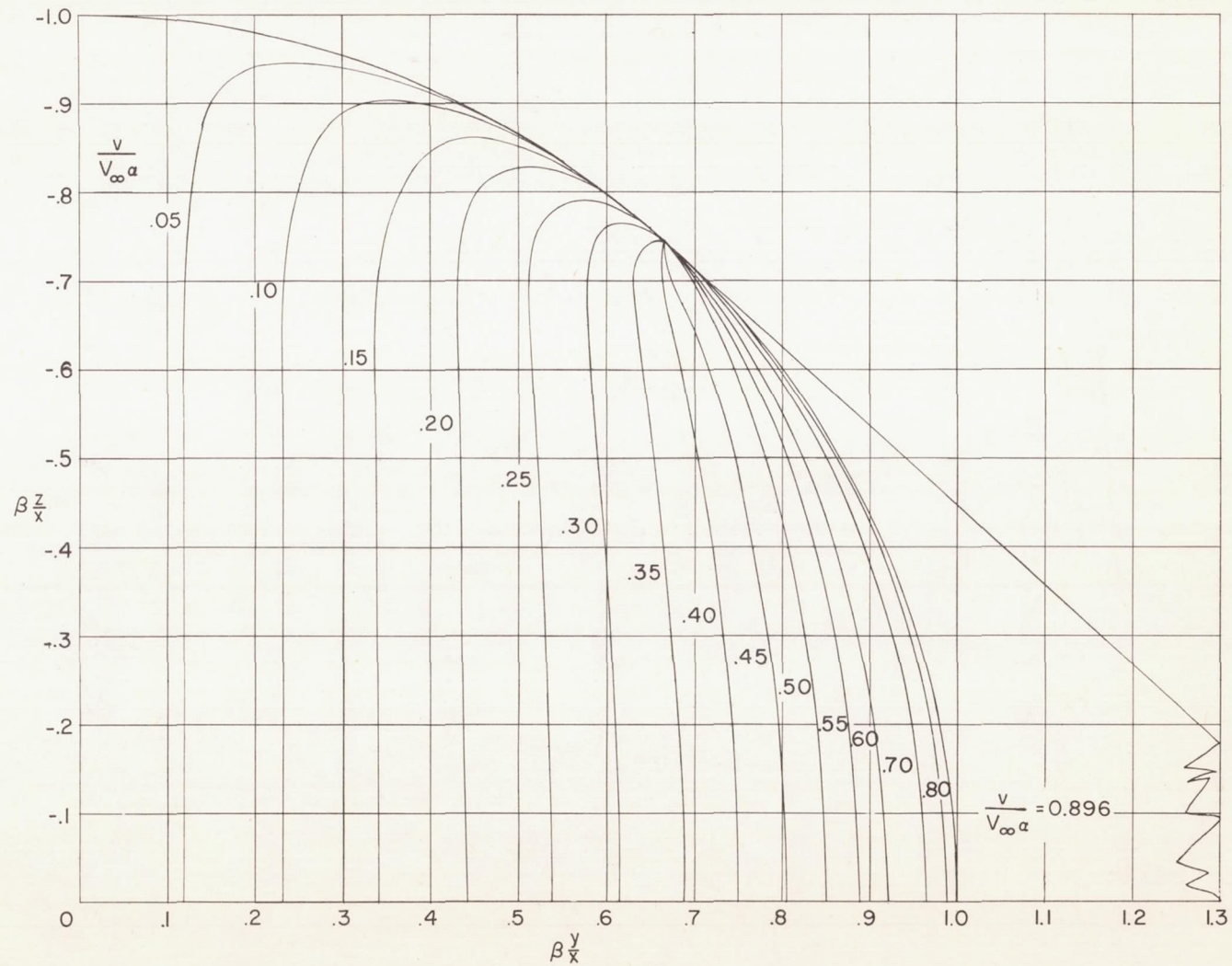
Figure 9.- Sidewash contours for a supersonic-leading-edge lifting triangular wing of infinite chord. $\beta m = 1.5$.
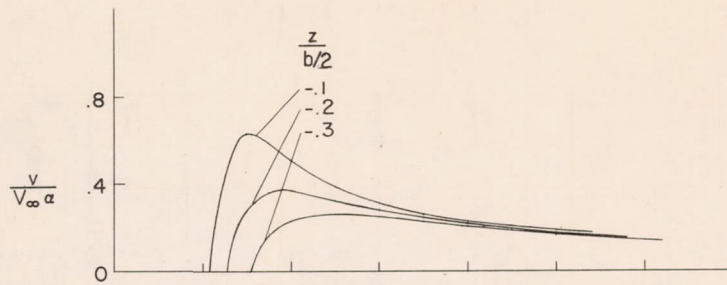
(a) $\dfrac{y}{b/2} = 0.25.$
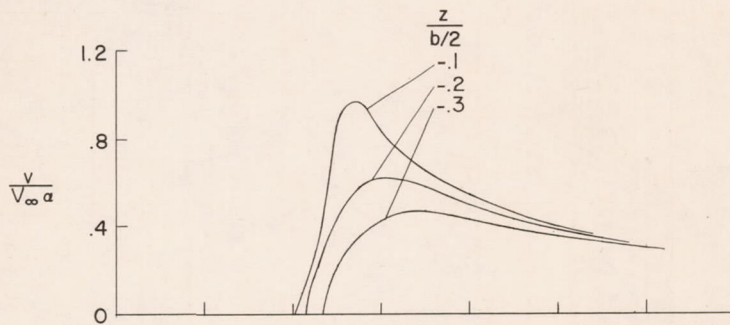
(b) $\dfrac{y}{b/2} = 0.50.$

(c) $\dfrac{y}{b/2} = 0.75.$

Figure 10.- Chordwise variation of sidewash at three spanwise positions and three vertical heights for a subsonic leading edge. $\beta m = 0.8.$
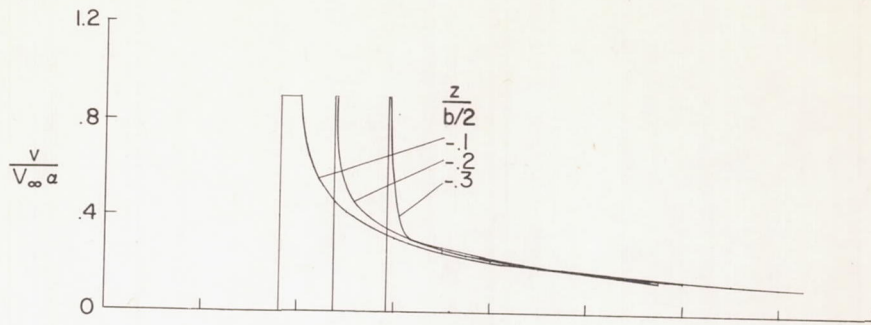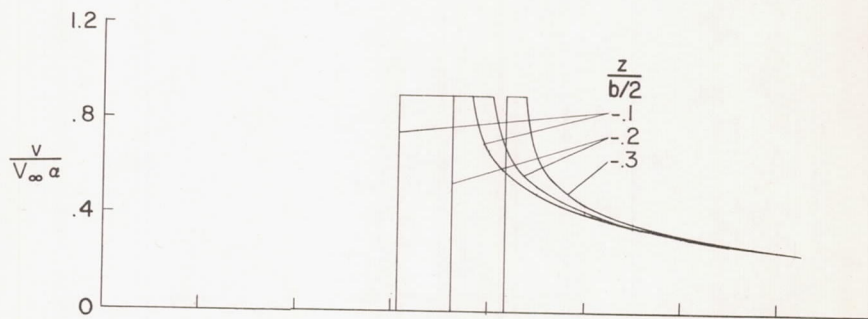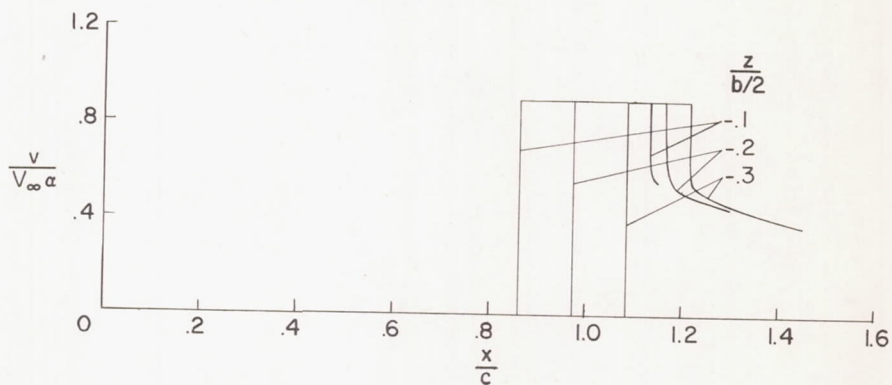
(a) $\dfrac{y}{b/2} = 0.25.$

(b) $\dfrac{y}{b/2} = 0.50.$

(c) $\dfrac{y}{b/2} = 0.75.$

Figure 11.- Chordwise variation of the conical part of the sidewash at three spanwise positions and three vertical heights for a supersonic leading edge. $\beta m = 1.5.$

Figure 12.- Two paths of integration for obtaining the velocity potential and associate notation.